Supporting Information for

Deconvoluting Capping Ligand Influence on Photophysical Properties in Tetrathiafulvalene-Based Diradicaloids

Nathan E. Lopez,[†a] Lauren E. McNamara,[†a] Sophie W. Anferov,[a] and John S. Anderson[a]

[a]Department of Chemistry, University of Chicago, Chicago, IL, USA

Correspondence to: jsanderson@uchicago.edu

Table of Contents

General Synthetic Methods 5

Characterization and Analysis Methods 5

Synthetic Procedures 6

Synthesis of $Pt(P(O\text{-}p\text{-}CF_3Ph)_3)_2Cl_2$ 6

Synthesis of $Pt(P(O\text{-}o\text{-}CH_3Ph)_3)_2Cl_2$ 6

Synthesis of $[\{NBDPt\}_2TTFtt][BAr^F{}_4]_2$ (**1**) 6

Synthesis of $[\{HEXPt\}_2TTFtt][BAr^F{}_4]_2$ (**2**) 6

Synthesis of $[\{Me_2CODPt\}_2TTFtt][BAr^F{}_4]_2$ (**3**) 7

Synthesis of $[\{(P(O\text{-}p\text{-}CF_3Ph)_3)_2Pt\}_2TTFtt][BAr^F{}_4]_2$ (**4**) 7

Synthesis of $[\{(P(OPh)_3)_2Pt\}_2TTFtt][BAr^F{}_4]_2$ (**5**) 7

Synthesis of $[\{(P(O\text{-}o\text{-}CH_3Ph)_3)_2Pt\}_2TTFtt][BAr^F{}_4]_2$ (**6**) 8

NMR Spectroscopy 8

^{1}H NMR spectra 8

Figure S1. ^{1}H NMR of $Pt(P(O\text{-}p\text{-}CF_3Ph)_3)_2Cl_2$ in CD_2Cl_2 8

Figure S2. ^{1}H NMR of $Pt(P(O\text{-}o\text{-}CH_3Ph)_3)_2Cl_2$ in CD_2Cl_2. 9

Figure S3. ^{1}H NMR of **1** in CD_2Cl_2. 9

Figure S4. ^{1}H NMR of **2** in CD_2Cl_2. 10

Figure S5. ^{1}H NMR of **3** in CD_2Cl_2. 10

Figure S6. ^{1}H NMR of **4** in CD_2Cl_2. 11

Figure S7. ^{1}H NMR of **5** in CD_2Cl_2. 11

Figure S8. ^{1}H NMR of **6** in CD_2Cl_2. 12

^{31}P NMR spectra 12

Figure S9. ^{31}P NMR of $Pt(P(O\text{-}p\text{-}CF_3Ph)_3)_2Cl_2$ in CD_2Cl_2. 12

Figure S10. ^{31}P NMR of $Pt(P(O\text{-}o\text{-}CH_3Ph)_3)_2Cl_2$ in CD_2Cl_2 13

Figure S11. ^{31}P NMR of **4** in CD_2Cl_2. 13

Figure S12. ^{31}P NMR of **5** in CD_2Cl_2. 14

Figure S13. ^{31}P NMR of **6** in CD_2Cl_2. 14

Evans method measurements 15

Figure S14. Evans method ^{1}H NMR spectrum of 7 mM solution of **1** in CD_2Cl_2. 15

Figure S15. Evans method ^{1}H NMR spectrum of 11 mM solution of **2** in CD_2Cl_2 15

Figure S16. Evans method ^{1}H NMR spectrum of 8 mM solution of **3** in CD_2Cl_2. 16

Figure S17. Evans method ^{1}H NMR spectrum of 20 mM solution of **4** in CD_2Cl_2. 16

Figure S18. Evans method ^{1}H NMR spectrum of 20 mM solution of **5** in CD_2Cl_2 17

Figure S19. Evans method ^{1}H NMR spectrum of 20 mM solution of **6** in CD_2Cl_2 17

Infrared Spectra 18
Figure S20. Infrared transmittance spectrum of a dropcast DCM solution of **1**. 18
Figure S21. Infrared transmittance spectrum of a dropcast DCM solution of **2**. 19
Figure S22. Infrared transmittance spectrum of a dropcast DCM solution of **3**. 19
Figure S23. Infrared transmittance spectrum of a dropcast DCM solution of **4**. 20
Figure S24. Infrared transmittance spectrum of a dropcast DCM solution of **5**. 20
Figure S25. Infrared transmittance spectrum of a dropcast DCM solution of **6**. 21
Photoluminescence Quantum Yield 21
Figure S26. Photoluminescence quantum yield determinations for **1** in DCM at 298 K.. 21
Figure S27. Photoluminescence quantum yield determinations for **2** in DCM at 298 K.. 22
Figure S28. Photoluminescence quantum yield determinations for **3** in DCM at 298 K 22
Figure S29. Photoluminescence quantum yield determinations for **4-6** in DCM at 298 K. 23
Photoluminescence Spectra in CD_2Cl_2 23
Figure S30. Photoluminescence spectrum of **3** in CD_2Cl_2. 23
Figure S31. Photoluminescence spectrum of **5** in CD_2Cl_2. 24
Figure S32. Photoluminescence spectrum of **6** in CD_2Cl_2. 24
Electron Paramagnetic Resonance (EPR) Spectra 25
Figure S33. X-Band EPR spectrum of **1** in DCM at 298 K. 25
Figure S34. X-Band EPR spectrum of **2** in DCM at 298 K. 25
Figure S35. X-Band EPR spectrum of **3** in DCM at 298 K. 26
Figure S36. X-Band EPR spectrum of **4** in DCM at 298 K. 26
Figure S37. X-Band EPR spectrum of **5** in DCM at 298 K. 27
Figure S38. X-Band EPR spectrum of **6** in DCM at 298 K. 27
X-Ray Crystallographic Data 28
Figure S39. SXRD of asymmetric unit of **1**. Pt, S, C. 28
Table S1. SXRD of **1**. 28
Figure S40. SXRD of asymmetric unit of **2**. Pt, S, C. Hydrogens, solvent, and counter anions omitted for clarity. 29
Figure S41. SXRD of entire molecule of **2** to show inversion symmetry. Pt, S, C. Hydrogens, solvent, and counter anions omitted for clarity. 29
Table S2. SXRD of **2**. 29
Figure S42. SXRD of asymmetric unit of **3**. Pt, S, C. Hydrogens, solvent, and counter anions omitted for clarity. 30
Table S3. SXRD of **3**. 30
Figure S43. SXRD of asymmetric unit of **4**. Pt, S, C, P, O, F. Hydrogens, solvent, and counter anions omitted for clarity. 31

Table S4. SXRD of **4**. 32

Figure S44. SXRD of asymmetric unit of **5**. Pt, S, C, P, O. Hydrogens, solvent, and counter anions omitted for clarity. 33

Table S5. SXRD of **5**. 33

Figure S45. SXRD of **6**. Pt, S, C, P, O. Hydrogens, solvent, and counter anions omitted for clarity. 34

Table S6. SXRD of **6**. 34

Computational Information 35

Computational Methods 35

2nd Order Perturbative Energy Analysis 35

Table S7. Computed backbonding and σ donation values and photophysical parameters for compounds **1-6** and select phosphine complexes previously reported. 36

Figure S46. Weighted absorption fit with 1 standard deviation. Fit including **4** and excluding **4** as an outlier. 37

Figure S47. Weighted emission energy fit with 1 standard deviation. Fit including **4** and excluding **4** as an outlier. 37

Figure S48. Absorption and emission of compounds **1-6** and select phosphine-capped PtTTFtt compounds plotted against only computed backbonding strength. 38

Figure S49. Absorption and emission of P-based ligands against computed backbonding (**4-6** and phosphine-capped PtTTFtt compounds) and a linear fit. 38

General Synthetic Methods

All syntheses were performed under dry N_2 in an MBraun UNIlab glovebox. Midwest Microlabs conducted all elemental analyses (C, H, N). All solvents were dried and N_2-purged on a Pure Process Technology solvent system, filtered through activated alumina, and stored over 4 Å molecular sieves. $TTFtt(SnBu_2)_2$,[1] $[Fc^{BzO}][BAr^F{}_4]$,[1] $P(O\text{-}o\text{-}CH_3Ph)_3$,[2] $Pt\{P(O\text{-}p\text{-}CF_3Ph)_3\}_2Cl_2$,[3] $Pt\{P(O\text{-}o\text{-}CH_3Ph)_3\}_2Cl_2$,[3] $Pt(NBD)Cl_2$,[4] $Pt(HEX)Cl_2$,[4] and $Pt(Me_2COD)Cl_2$[4] were prepared according to literature procedures (NBD = 2,5-norbornadiene, HEX = 1,5-hexadiene, and Me_2COD = (1,5-dimethyl-1,5-cyclooctadiene). All other chemicals and reagents were purchased from commercial sources and used as received.

Characterization and Analysis Methods

NMR Spectroscopy. ^1H and ^{31}P spectra were acquired on Bruker DRX 400 spectrometers. Residual solvent peaks were referenced for all ^1H NMR experiments and 85% phosphoric acid was used as a reference for ^{31}P NMR measurements. Evans method experiments were conducted in CD_2Cl_2 with a capillary of 90%/10% w/w CD_2Cl_2/CH_2Cl_2. Diamagnetic corrections were applied using Pascal's constants.[5]

Fourier Transform Infrared (FT-IR) Spectroscopy. FT-IR measurements were collected by drop-casting DCM solutions onto KBr plates. Each spectrum was collected on a Bruker Tensor II. All samples were baseline and background corrected in the OPUS software.

UV-Vis-NIR. UV–vis–NIR measurements were collected using a Shimadzu UV-3600 Plus dual-beam spectrophotometer and a Thermo Scientific Evolution 300 spectrometer.

Photoluminescence Spectroscopy. Room-temperature emission spectra were collected on a Horiba Scientific PTI QuantaMaster fluorometer.

Photoluminescence Quantum Yield Determination. Samples in 1 cm quartz fluorescence cuvettes were normalized to optical densities at 900 nm using UV-vis-NIR measurements. To minimize reabsorption effects, all samples were kept under 0.1 optical density (OD) at 900 nm. ODs at 900 nm were plotted against integrated photoluminescence. The reference compound used was $[(dppePt)_2TTFtt][BAr^F{}_4]_2$ with PLQY = 0.136% in CH_2Cl_2 at 298 K.[6] Individual quantum yields were calculated according to the following equation: $\phi_s = \phi_r \left(\frac{m_s}{m_r}\right)\left(\frac{n_s}{n_r}\right)^2$ where ϕ is the photoluminescence quantum yield (PLQY), m is the gradient of the OD vs integrated PL plot, *n* is the index of refraction of the solvent, and *r* and *s* refer to the reference and sample, respectively.

EPR Spectroscopy. EPR spectra were recorded on a Bruker Elexsys E500 spectrometer.

Single-crystal X-Ray Diffraction. The diffraction data for **1-6** were measured at 100 K on a Bruker D8 VENTURE with PHOTON 100 CMOS detector system equipped with a Cu and Mo-target micro-focus X-ray tube (λ = 1.54184 Å and 0.71073 Å respectively). Data reduction and integration were performed with the Bruker APEX3 software package (Bruker AXS, version 2015.5-2, 2015). Data was scaled and corrected for absorption effects using the multi-scan procedure as implemented in SADABS (Bruker AXS, version 2014/5, 2015, part of Bruker APEX3 software package). The structure was solved by the dual method implemented in SHELXT[7] and refined by a full-matrix least-squares procedure using OLEX23[8] software package (XL refinement program version 2014/7[9]). Suitable crystals were mounted on a cryo-loop and transferred into the cold nitrogen stream of the Bruker D8 Venture diffractometer. C–H hydrogen atoms were generated by geometrical considerations, constrained to idealized geometries, and allowed to ride on their carrier atoms with an isotropic displacement parameter related to the equivalent displacement parameter of their carrier atoms.

We note A- and B-level alerts for these compounds, likely resulting both from the presence of a twin from overlapping plates of crystals, the propensity of the $BAr^F_4^-$ anions to disorder, and the high electron density characteristic of Pt-centers which leads to spurious peaks in the density map. We note that these were the best diffracting samples among numerous crystallization attempts, and particularly **2** and **4** are best regarded structures which provide only connectivity. Given the propensity of the anion to disorder, not the central TTF core, we note that bond lengths for the central C–C bond in **1**, **2**, **3**, and **5**, and **6** still have high enough resolution to be compare with predictions and previous work.

Synthetic Procedures

Synthesis of $Pt(P(O\text{-}p\text{-}CF_3Ph)_3)_2Cl_2$

To an oven-dried two-neck flask equipped with magnetic stir bar, N_2 inlet, and rubber septum, $Pt(COD)Cl_2$ (0.200 g, 0.53 mmol) was dissolved in 5 mL of dry DCM. To this, $P(O\text{-}p\text{-}CF_3Ph)_3$ (0.546 g, 1.06 mmol) was added and the reaction mixture was stirred for 6 h at room temperature. The reaction was then concentrated to 1 mL and hexanes were added slowly to form a white precipitate. The precipitate was then collected *via* vacuum filtration (0.545 g, 80%). ^1H NMR (400 MHz, CD_2Cl_2, 298 K) δ 7.27 (d, Ar-H), 7.64 (d, Ar-H). $^{31}P\{^1H\}$ NMR (162 MHz, CD_2Cl_2, 298 K) δ 60.75 ($J_{Pt\text{-}P}$ = 2863 Hz). Anal. Calcd for $Pt(P(O\text{-}p\text{-}CF_3Ph)_3)_2Cl_2$, $C_{42}H_{24}O_6F_{18}P_2PtCl_2$: C 38.97%, H 1.87%, N 0%; found: C 38.92%, H 2.05%, N none.

Synthesis of $Pt(P(O\text{-}o\text{-}CH_3Ph)_3)_2Cl_2$

To an oven-dried two-neck flask equipped with magnetic stir bar, N_2 inlet, and rubber septum, $Pt(COD)Cl_2$ (0.150 g, 0.4 mmol) was dissolved in 5 mL of dry DCM. To this, $P(O\text{-}o\text{-}CH_3Ph)_3$ (0.282 g, 0.8 mmol) was added and the reaction mixture was stirred for 6 h at room temperature. The reaction was then concentrated to 1 mL and hexanes were added slowly and white precipitate formed. The precipitate was collected *via* vacuum filtration (0.176 g, 45%). ^1H NMR (400 MHz, CD_2Cl_2, 298 K) δ 2.08 (s, CH_3), 7.09-7.20 (m, Ar-H), 7.34 (m, Ar-H). $^{31}P\{^1H\}$ NMR (162 MHz, CD_2Cl_2, 298 K) δ 56.83 ($J_{Pt\text{-}P}$ = 2929 Hz). Anal. Calcd for $Pt(P\text{-}o\text{-}CH_3Ph)_3)_2Cl_2$, $C_{42}H_{42}O_6P_2PtCl_2$: C 51.96%, H 4.37%, N 0%; found: C 51.89%, H 4.55%, N none.

Synthesis of $[\{NBDPt\}_2TTFtt][BAr^F_4]_2$ (**1**)

$TTFtt(SnBu_2)_2$ (0.016 g, 0.02 mmol) was dissolved in 2 mL DCM and added dropwise to a solution of $Pt(NBD)Cl_2$ (0.015 g 0.04 mmol) in 2 mL of DCM. The mixture turned deep red-orange, and the suspension was allowed to stir for 10 min. Then, $[Fc^{BzO}][BAr^F_4]$ (0.050 mg 0.04 mmol) in 3 mL DCM was added slowly to the reaction mixture. The reaction slowly turned from dark red-orange to green-brown and after stirring for 5 min, the solution was concentrated to 1 mL under vacuum. While stirring, 5 mL petroleum ether was added slowly, and dichroic green-brown crystals formed. The crystals were washed with petroleum ether (3x5 mL) and dried under vacuum. The crude product was redissolved in 1 mL of DCM, filtered through celite, and layered with petroleum ether. The layered solution was placed in a −35 °C freezer and allowed to recrystallize overnight, yielding dichroic green-brown crystals (0.040 g, 70%) suitable for SXRD. ^1H NMR (400 MHz, CD_2Cl_2, 298 K) δ 1.92 (bm, NBD 7-H), 4.40 (bm, NBD 1-H, 4-H), 5.63 (bm, NBD =CH), 7.55 (bs, $[BAr^F_4]^-$), 7.72 (bs, $[BAr^F_4]^-$). We note due to the air-sensitive nature of this compound, we did not run elemental analysis. See NMR and crystal structure for purity and composition/connectivity, respectively.

Synthesis of $[\{HEXPt\}_2TTFtt][BAr^F_4]_2$ (**2**)

$TTFtt(SnBu_2)_2$ (0.065 g, 0.08 mmol) was dissolved in 3 mL DCM and added dropwise to a solution of $Pt(HEX)Cl_2$ (0.057 g, 0.16 mmol) in 3 mL of DCM. The mixture turned deep red-brown, and the suspension was allowed to stir for 10 min. Then, $[Fc^{BzO}][BAr^F_4]$ (0.200 g, 0.17 mmol) in 4 mL DCM was added slowly to the reaction mixture. The reaction slowly turned from dark red-brown to green-brown and after stirring

for 5 min, the solution was concentrated to 1 mL under vacuum. While stirring, 5 mL petroleum ether was added slowly, and dichroic blue-brown crystals formed. The crystals were washed with petroleum ether (3x5 mL) and dried under vacuum. The crude product was redissolved in 2 mL of DCM, filtered through celite, and layered with petroleum ether. The layered solution was placed in a -35 °C freezer and allowed to recrystallize overnight, yielding dichroic blue-brown crystals (0.146 g, 69%) suitable for SXRD. ^{1}H NMR (400 MHz, CD_2Cl_2, 298 K) δ 2.80 (bm, HEX CH_2), 4.26-4.30 (bd, HEX =CH_2 (Z)), 5.07 (bd, HEX =CH_2 (E)), 5.93 (bm, HEX =CH), 7.57 (s, [BAr^F_4]$^-$), 7.73 (s, [BAr^F_4]$^-$). Anal. Calcd for **2**, $C_{82}H_{44}B_2F_{48}Pt_2S_8$: C 37.74%, H 1.70%, N 0%; found: C 37.73%, H 1.87%, N none.

Synthesis of [{Me_2CODPt}$_2$TTFtt][BAr^F_4]$_2$ (**3**)

TTFtt($SnBu_2$)$_2$ (0.050 g, 0.06 mmol) was dissolved in 3 mL DCM and added dropwise to a solution of Pt(Me_2COD)Cl_2 (0.051 g 0.13 mmol) in 3 mL of DCM. The solution turned dark brown, and was allowed to stir for 10 min. Then, [Fc^{BzO}][BAr^F_4] (0.175 g 0.15 mmol) in 4 mL DCM was added slowly to the dark brown solution. The reaction slowly turned from dark brown to green and after stirring for 5 min, the solution was concentrated to 1 mL under vacuum. While stirring, 5 mL petroleum ether was added slowly, and green crystals formed. The crystals were washed with petroleum ether (3x5 mL) and dried under vacuum. The crude product was redissolved in 2 mL of DCM, filtered through celite, and layered with hexanes. The layered solution was placed in a −35 °C freezer and allowed to recrystallize for two months, yielding green crystals (0.088 g, 52%) suitable for SXRD. ^{1}H NMR (400 MHz, CD_2Cl_2, 298 K) δ 2.14 (bs, Me_2COD CH_3), 2.48 (bm, Me_2COD CH_2), 2.55 (bm, Me_2COD CH_2), 2.71 (bm, Me_2COD CH_2), 5.54 (bm, Me_2COD =CH), 7.56 (s, [BAr^F_4]$^-$), 7.72 (s, [BAr^F_4]$^-$). Anal. Calcd for **3**, $C_{90}H_{56}B_2F_{48}Pt_2S_8$: C 39.77%, H 2.08%, N 0%; found: C 40.10%, H 2.07%, N none.

Synthesis of [{(P(O-*p*-CF_3Ph)$_3$)$_2$Pt}$_2$TTFtt][BAr^F_4]$_2$ (**4**)

TTFtt($SnBu_2$)$_2$ (0.050 g, 0.06 mmol) was dissolved in 4 mL CH_2Cl_2 and added dropwise to a solution of Pt{P(O-*p*-CF_3Ph)$_3$}Cl_2 (0.155 g, 0.12 mmol) in 3 mL of CH_2Cl_2. The solution turned deep red and the suspension was allowed to stir for 10 min. Then, [Fc^{BzO}][BAr^F_4] (0.165 g, 0.132 mmol) in 4 mL CH_2Cl_2 was added slowly to the reaction mixture. The solution slowly turned from red to green and after stirring for 5 min, the solution was concentrated to 1 mL under vacuum. While stirring, 5 mL petroleum ether was added slowly, and green crystals formed. The crystals were washed with petroleum ether (3x3 mL) and dried under vacuum. The crude product was redissolved in 1 mL of CH_2Cl_2, filtered through celite, and layered with petroleum ether. The layered solution was placed in a −35 °C freezer and allowed to recrystallize overnight, yielding green crystals (0.235 g, 87%) suitable for SXRD. ^{1}H NMR (400 MHz, CD_2Cl_2, 298 K) δ 7.19 (d, Ar-H), 7.53 (s, [BAr^F_4]$^-$), 7.63 (d, Ar-H), 7.73 (s, [BAr^F_4]$^-$). ^{31}P{^{1}H} NMR (162 MHz, CD_2Cl_2, 298 K) δ 73.57 ($J_{Pt\text{-}P}$ = 2400 Hz). Anal. Calcd for **4**, $C_{154}H_{72}O_{12}P_4B_2F_{60}Pt_2S_8$: C 41.08%, H 1.62%, N 0%; found: C 41.38%, H 1.71%, N none.

Synthesis of [{(P(OPh)$_3$)$_2$Pt}$_2$TTFtt][BAr^F_4]$_2$ (**5**)

TTFtt($SnBu_2$)$_2$ (0.033 g, 0.04 mmol) was dissolved in 4 mL CH_2Cl_2 and added dropwise to a solution of Pt{P(OPh)$_3$}Cl_2 (0.078 g, 0.08 mmol) in 3 mL of CH_2Cl_2. The solution turned dark red and was allowed to stir for 10 min. Then, [Fc^{BzO}][BAr^F_4] (0.101 g, 0.088 mmol) in 4 mL CH_2Cl_2 was added slowly to the reaction mixture. The solution slowly turned from red to dark green and after stirring for 5 min, the solution was concentrated to 1 mL under vacuum. While stirring, 5 mL petroleum ether was added slowly and green crystals formed. The crystals were washed with petroleum ether (3x3 mL) and dried under vacuum. The crude product was redissolved in 1 mL of CH_2Cl_2, filtered through celite, and layered with petroleum ether. The layered solution was placed in a −35 °C freezer and allowed to recrystallize overnight, yielding green crystals (0.108 g, 73%) suitable for SXRD. ^{1}H NMR (400 MHz, CD_2Cl_2, 298 K) δ 7.07 (d, Ar-H), 7.29 (m,

Ar-H), 7.55 (s, [BAr$^{F}{}_{4}$]$^{-}$), 7.73 (s, [BAr$^{F}{}_{4}$]$^{-}$). ^{31}P{^{1}H} NMR (162 MHz, CD_2Cl_2, 298 K) δ 70.91. We note that we were not able to resolve J_{Pt-P} coupling for this compound. Anal. Calcd for 5, $C_{142}H_{84}O_{12}P_4B_2F_{48}Pt_2S_8$: C 46.26%, H 2.30%, N 0%; found: C 46.14%, H 2.54%, N none.

Synthesis of [{(P(O-*o*-CH_3Ph)$_3$)$_2$Pt}$_2$TTFtt][BAr$^{F}{}_{4}$]$_2$ (**6**)

TTFtt($SnBu_2$)$_2$ (0.050 g, 0.06 mmol) was dissolved in 4 mL CH_2Cl_2 and added dropwise to a solution of Pt{P(O-*o*-CH_3Ph)$_3$}Cl_2 (0.116 g, 0.12 mmol) in 3 mL of CH_2Cl_2. The solution turned deep purple and was allowed to stir for 10 min. Then, [Fc^{BzO}][BAr$^{F}{}_{4}$] (0.165 g, 0.132 mmol) in 4 mL CH_2Cl_2 was added slowly to the reaction mixture. The solution slowly turned from purple to green and after stirring for 5 min, the solution was concentrated to 1 mL under vacuum. While stirring, 5 mL petroleum ether was added slowly and green crystals formed. The crystals were washed with petroleum ether (3x3 mL) and dried under vacuum. The crude product was redissolved in 1 mL of CH_2Cl_2, filtered through celite, and layered with petroleum ether. The layered solution was placed in a −35 °C freezer and allowed to recrystallize overnight, yielding green crystals (0.171 g, 74%) suitable for SXRD. ^{1}H NMR (400 MHz, CD_2Cl_2, 298 K) δ 1.98 (s, CH_3), 7.01-7.17 (m, Ar-H), 7.55 (s, [BAr$^{F}{}_{4}$]$^{-}$), 7.73 (s, [BAr$^{F}{}_{4}$]$^{-}$). ^{31}P{^{1}H} NMR (162 MHz, CD_2Cl_2, 298 K) δ 68.86 (J_{Pt-P} = 2431 Hz). Anal. Calcd for **6**, $C_{154}H_{108}O_{12}P_4B_2F_{48}Pt_2S_8$: C 47.98%, H 2.83%, N 0%; found: C 48.08%, H 3.03%, N none.

NMR Spectroscopy

^{1}H NMR spectra

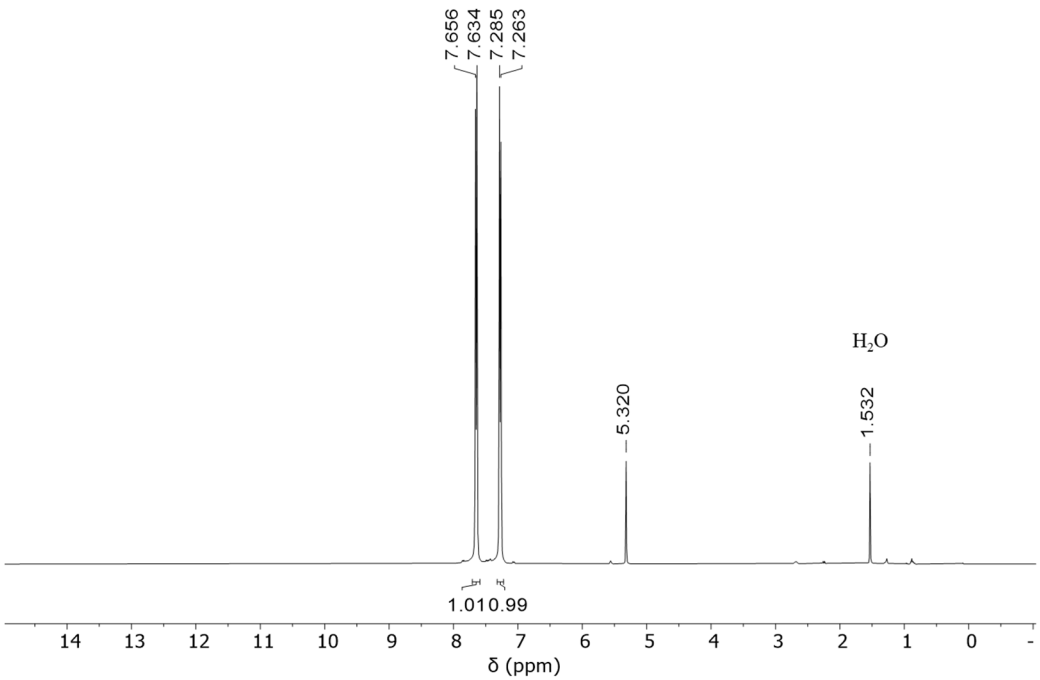

Figure S1. ^{1}H NMR of Pt(P(O-*p*-CF_3Ph)$_3$)$_2$$Cl_2$ in CD_2Cl_2.

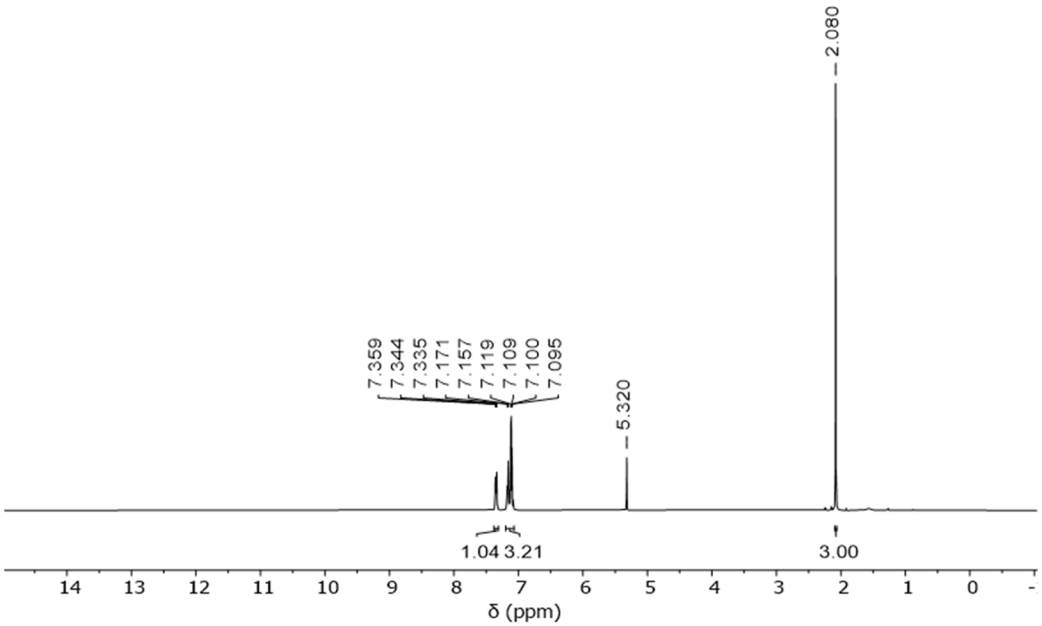

Figure S2. ^{1}H NMR of $Pt(P(O\text{-}o\text{-}CH_3Ph)_3)_2Cl_2$ in CD_2Cl_2.

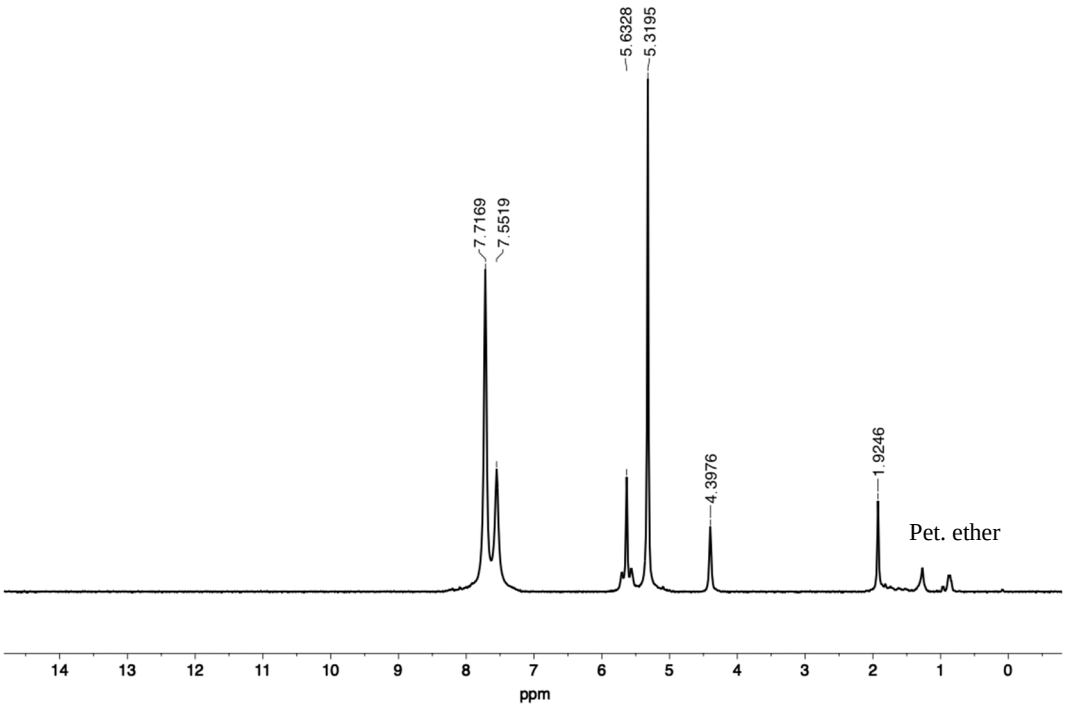

Figure S3. ^{1}H NMR of **1** in CD_2Cl_2.

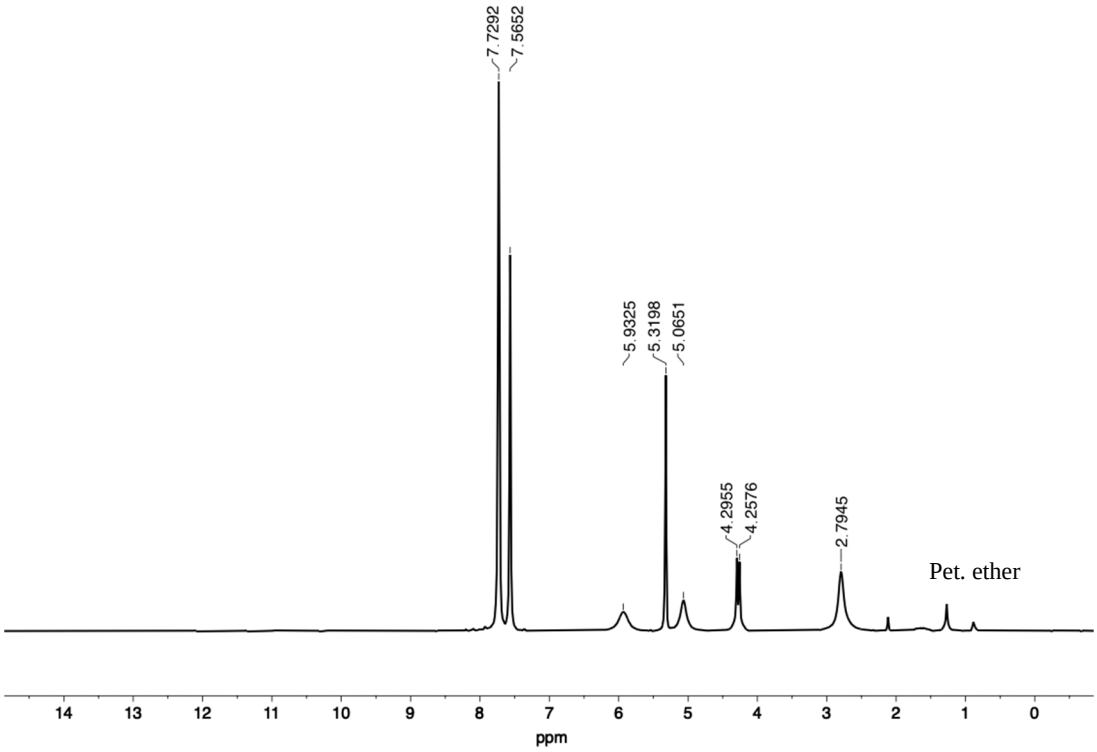

Figure S4. ^{1}H NMR of **2** in CD_2Cl_2.

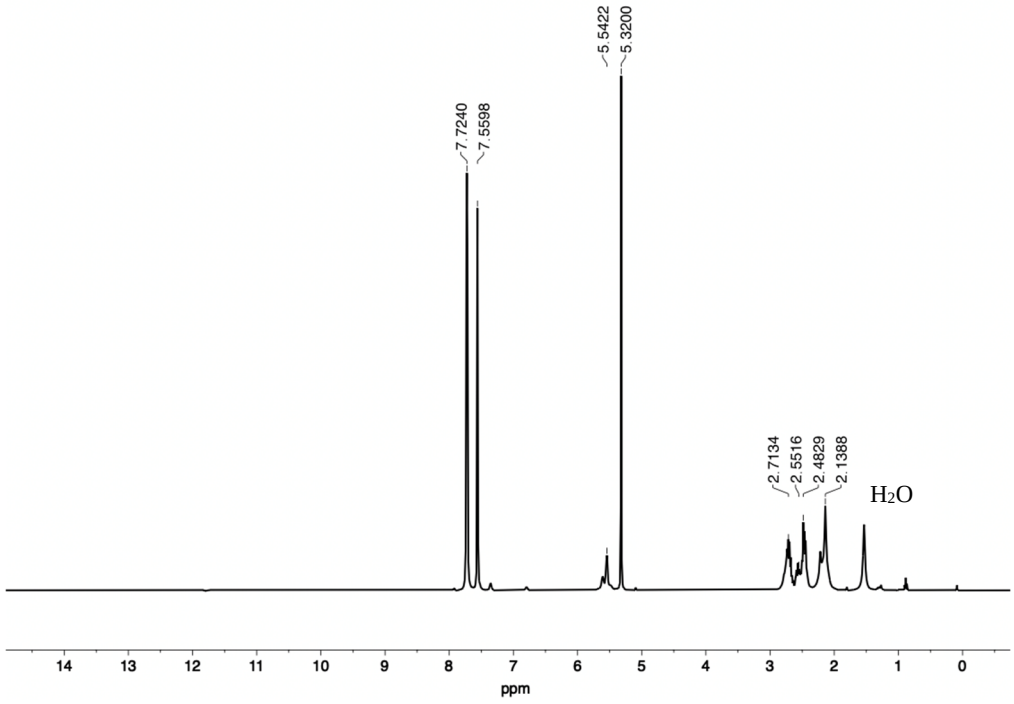

Figure S5. ^{1}H NMR of **3** in CD_2Cl_2.

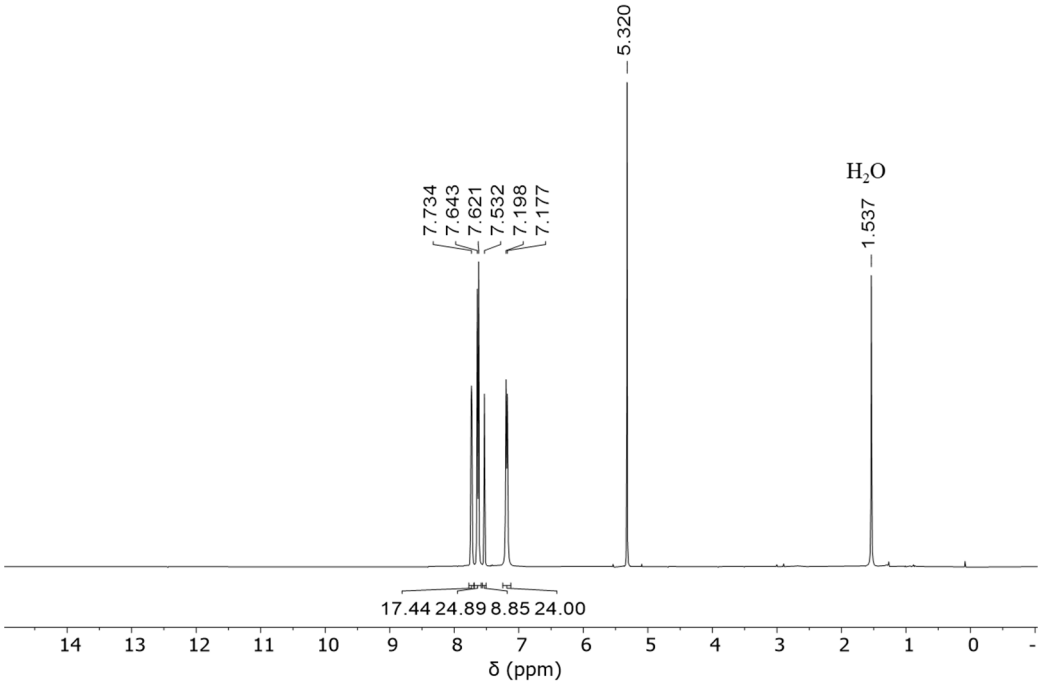

Figure S6. ^{1}H NMR of **4** in CD_2Cl_2.

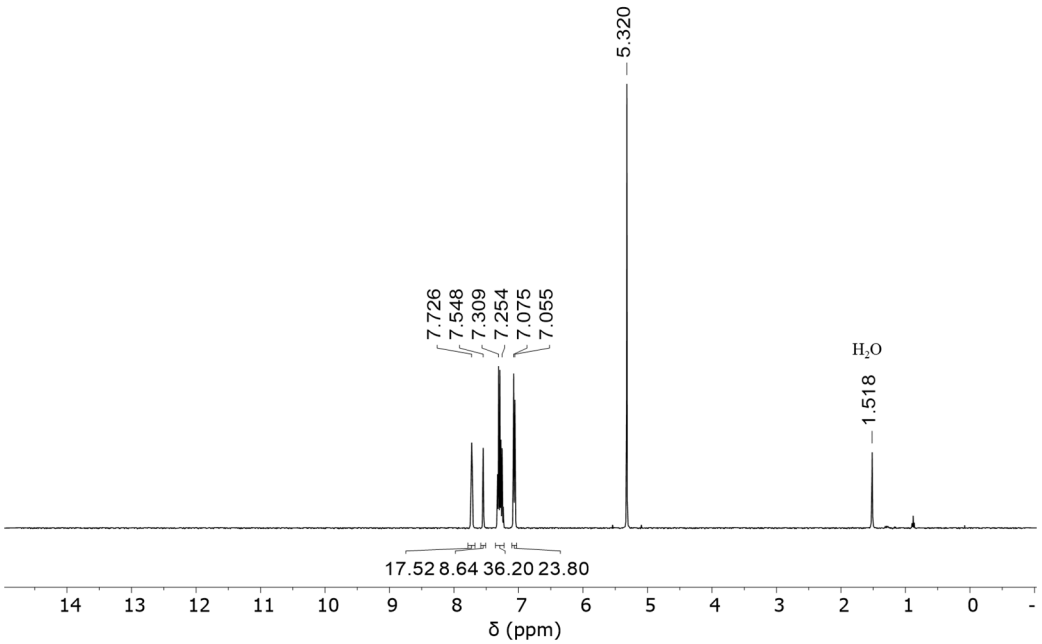

Figure S7. ^{1}H NMR of **5** in CD_2Cl_2.

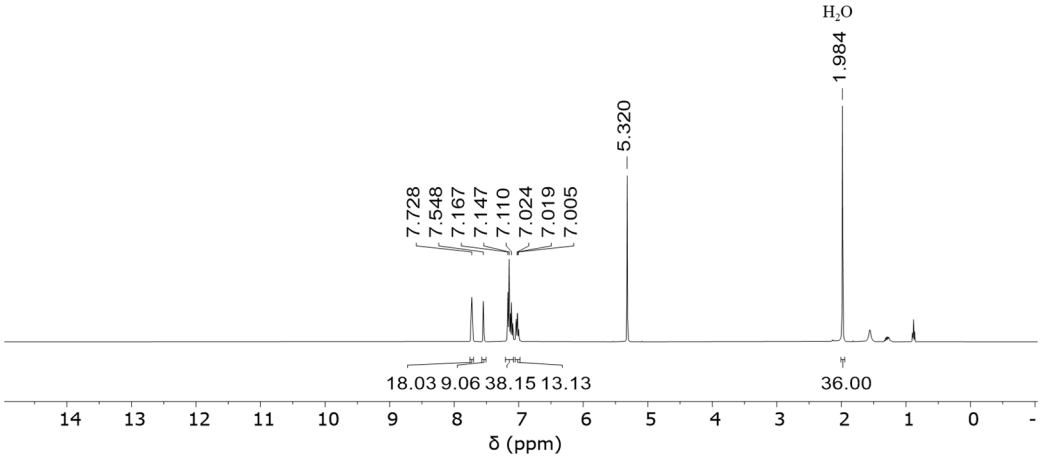

Figure S8. ^{1}H NMR of **6** in CD_2Cl_2.

^{31}P NMR spectra

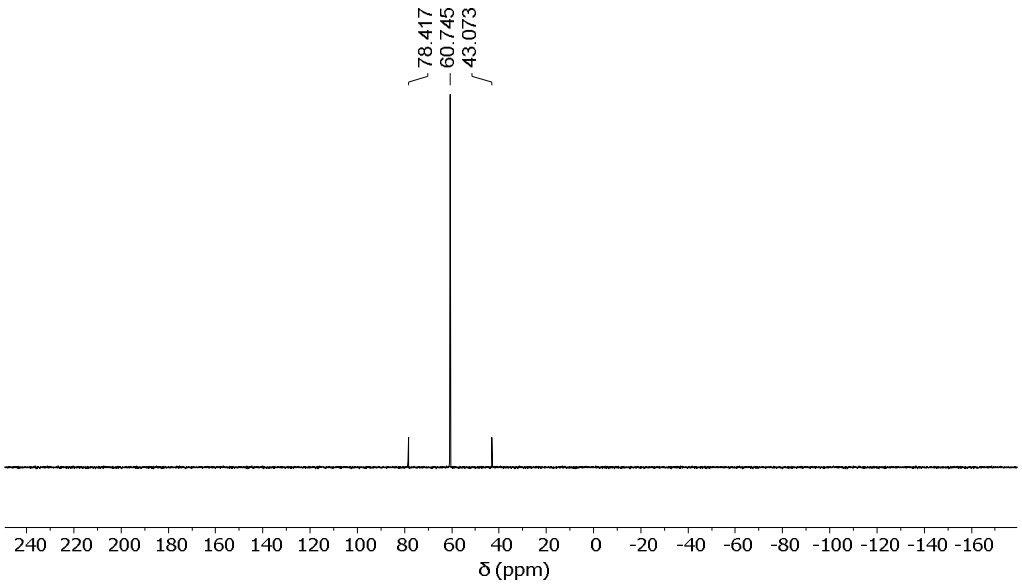

Figure S9. ^{31}P NMR of $Pt(P(O\text{-}p\text{-}CF_3Ph)_3)_2Cl_2$ in CD_2Cl_2.

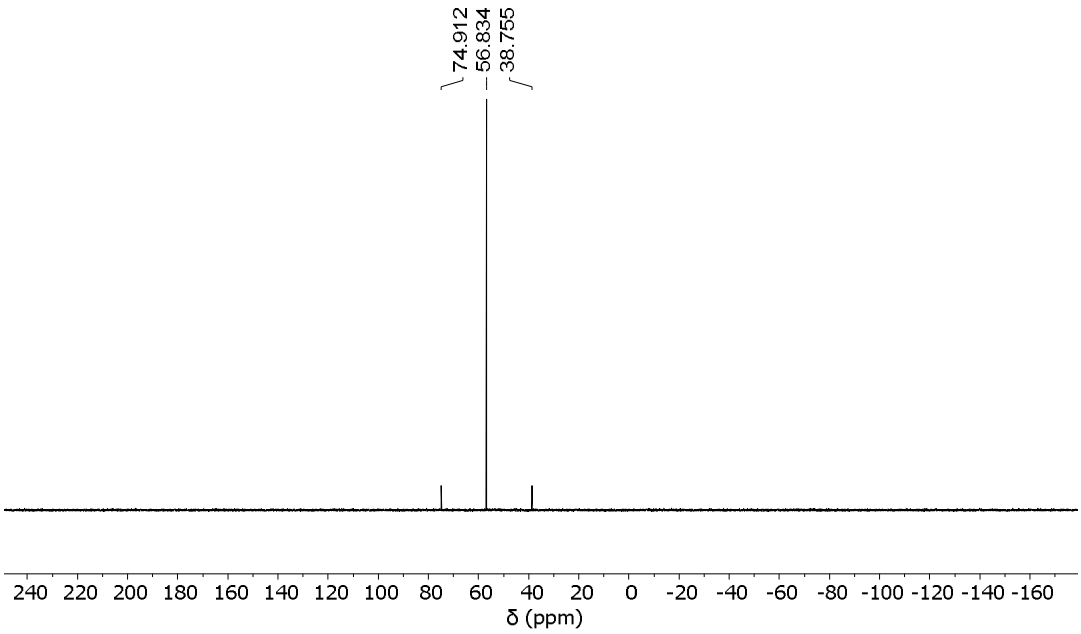

Figure S10. ^{31}P NMR of $Pt(P(O\text{-}o\text{-}CH_3Ph)_3)_2Cl_2$ in CD_2Cl_2.

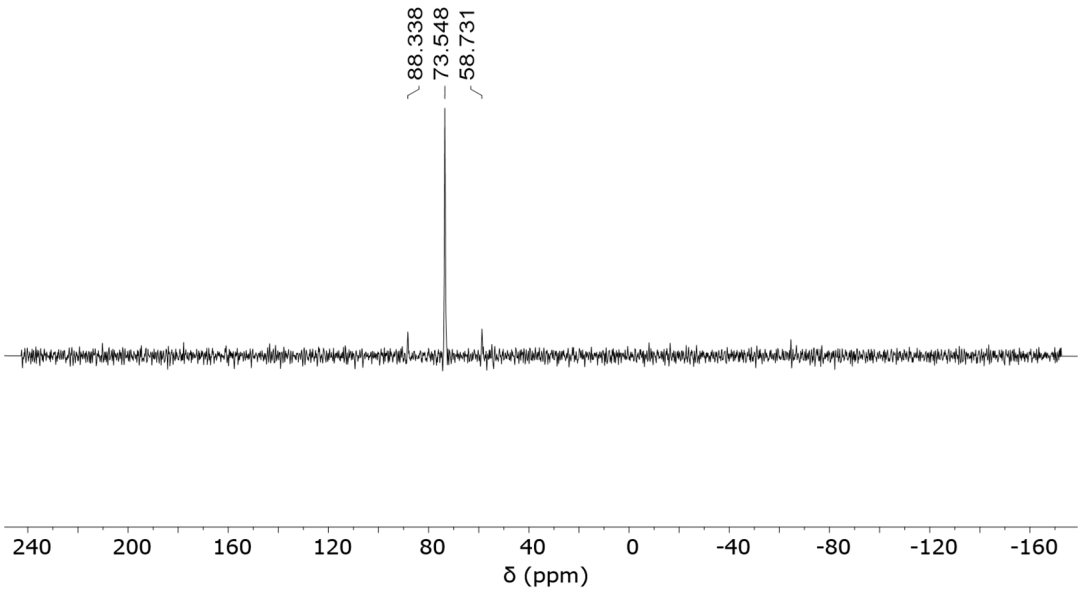

Figure S11. ^{31}P NMR of **4** in CD_2Cl_2.

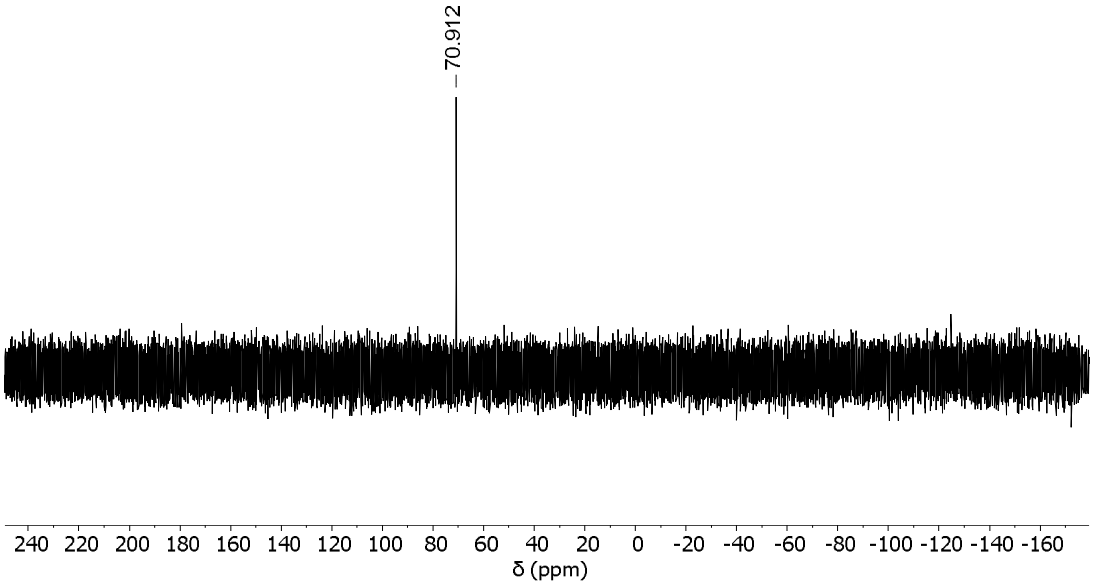

Figure S12. ^{31}P NMR of **5** in CD_2Cl_2.

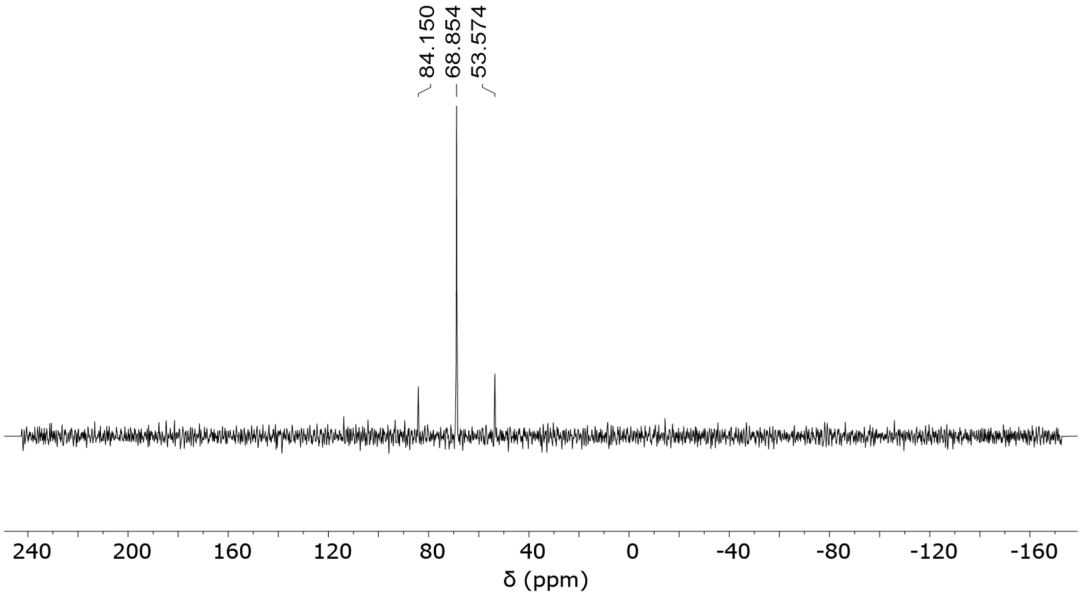

Figure S13. ^{31}P NMR of **6** in CD_2Cl_2.

Evans method measurements

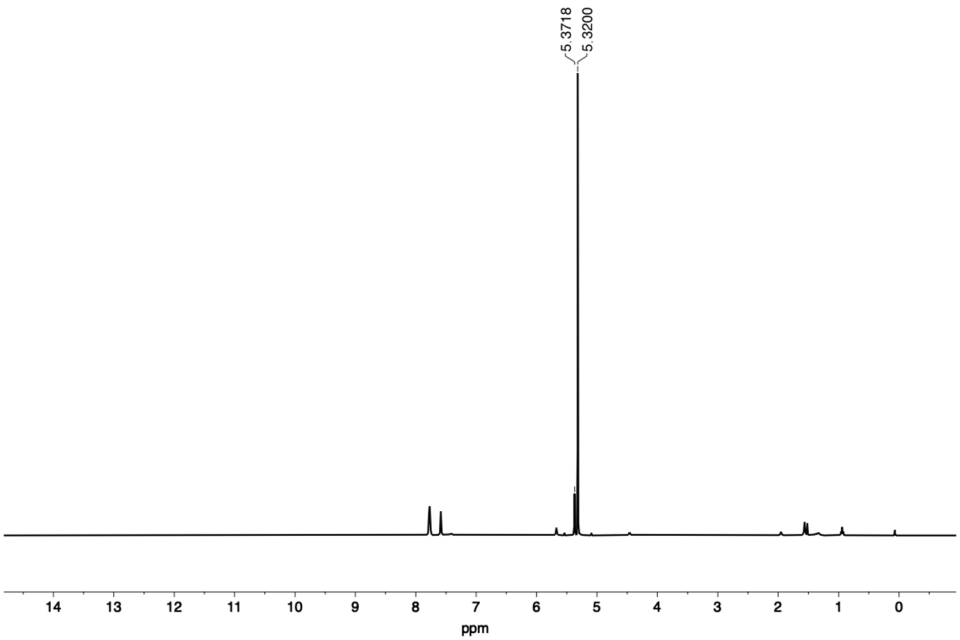

Figure S14. Evans method ^{1}H NMR spectrum of 7 mM solution of **1** in CD_2Cl_2. Magnetic moment: 2.05 μ_B.

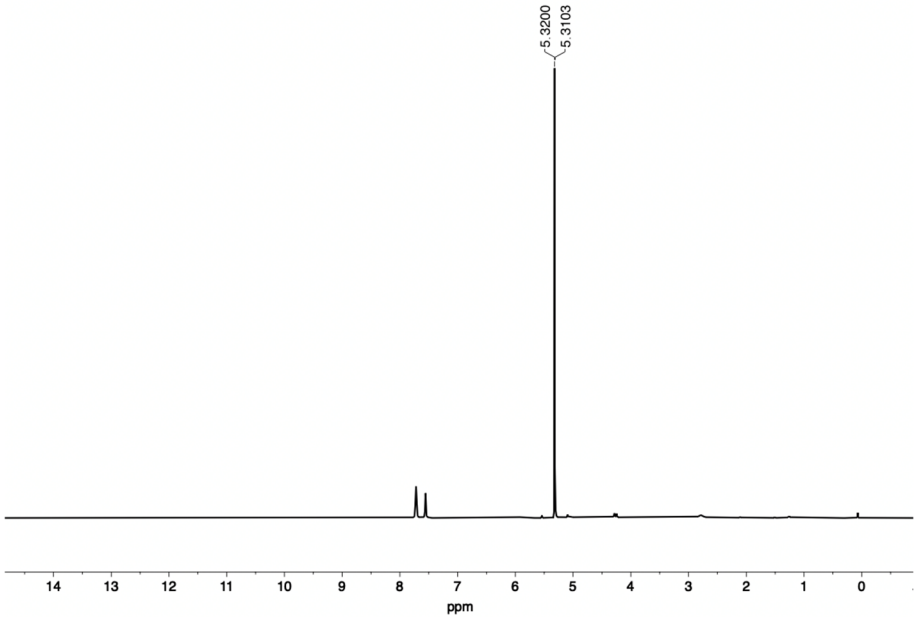

Figure S15. Evans method ^{1}H NMR spectrum of 11 mM solution of **2** in CD_2Cl_2. Magnetic moment: 0.88 μ_B.

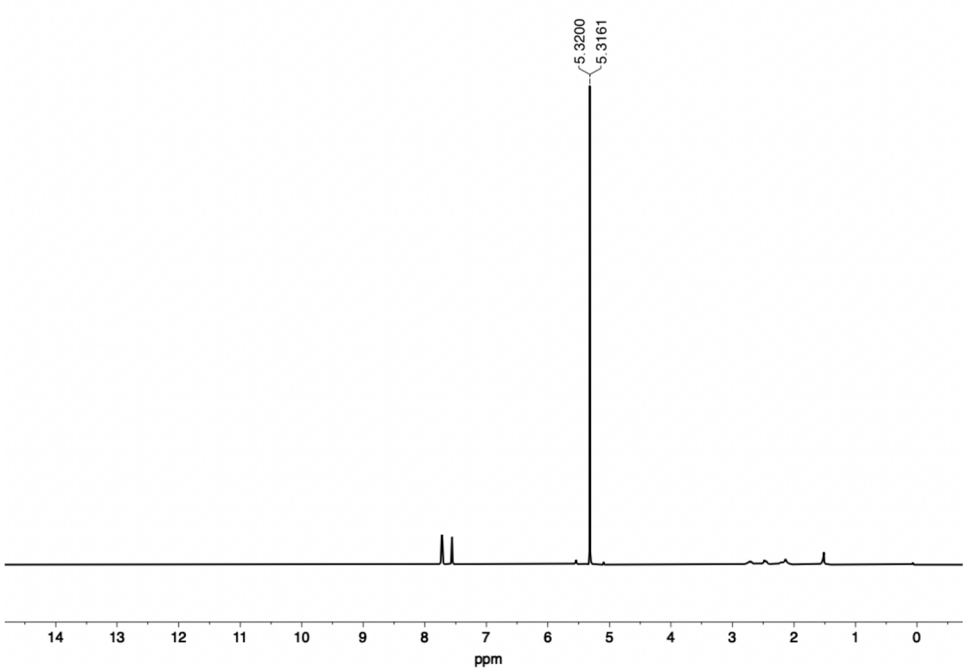

Figure S16. Evans method ^{1}H NMR spectrum of 8 mM solution of **3** in CD_2Cl_2. Magnetic moment: 0.79 μ_B.

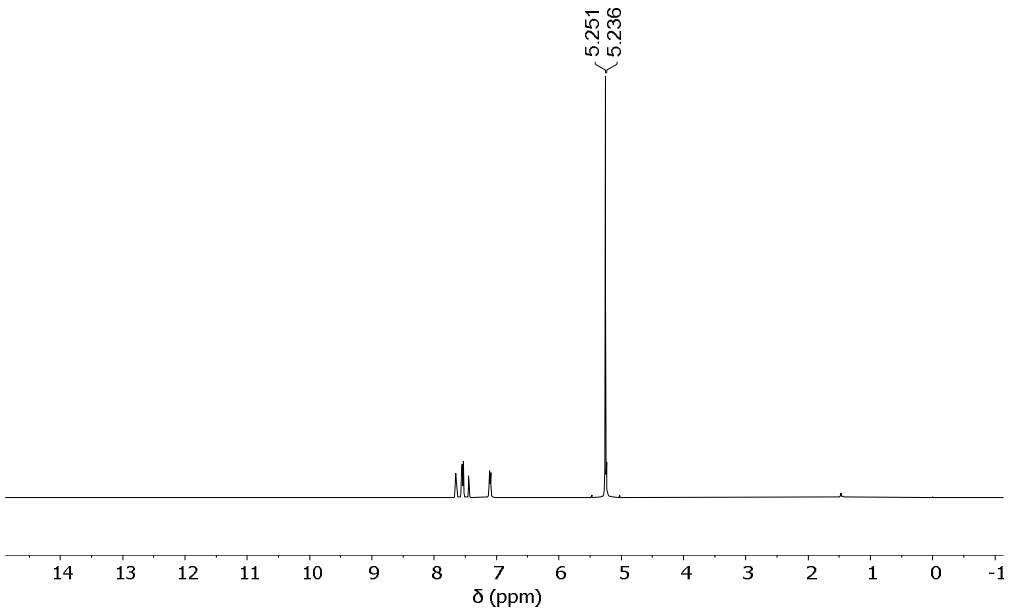

Figure S17. Evans method ^{1}H NMR spectrum of 20 mM solution of **4** in CD_2Cl_2. Magnetic moment: 1.20 μ_B.

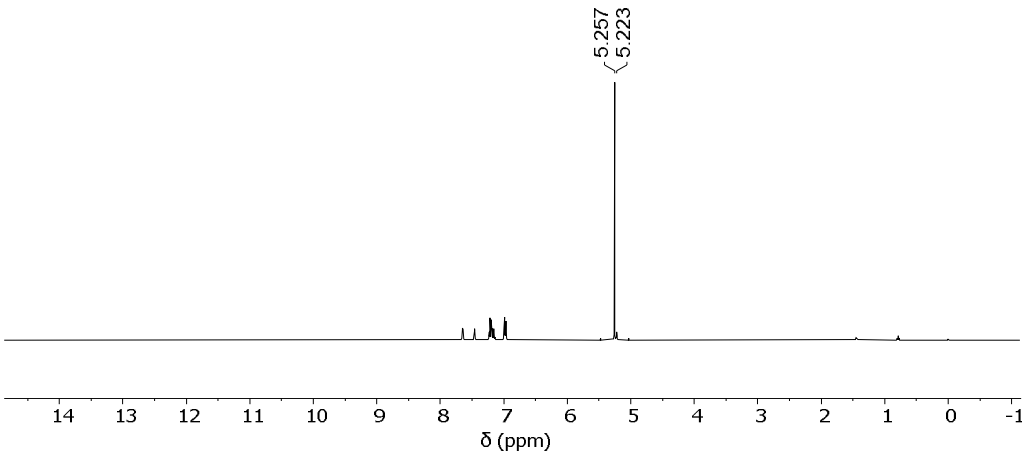

Figure S18. Evans method ^{1}H NMR spectrum of 20 mM solution of **5** in CD_2Cl_2. Magnetic moment: 1.27 μ_B.

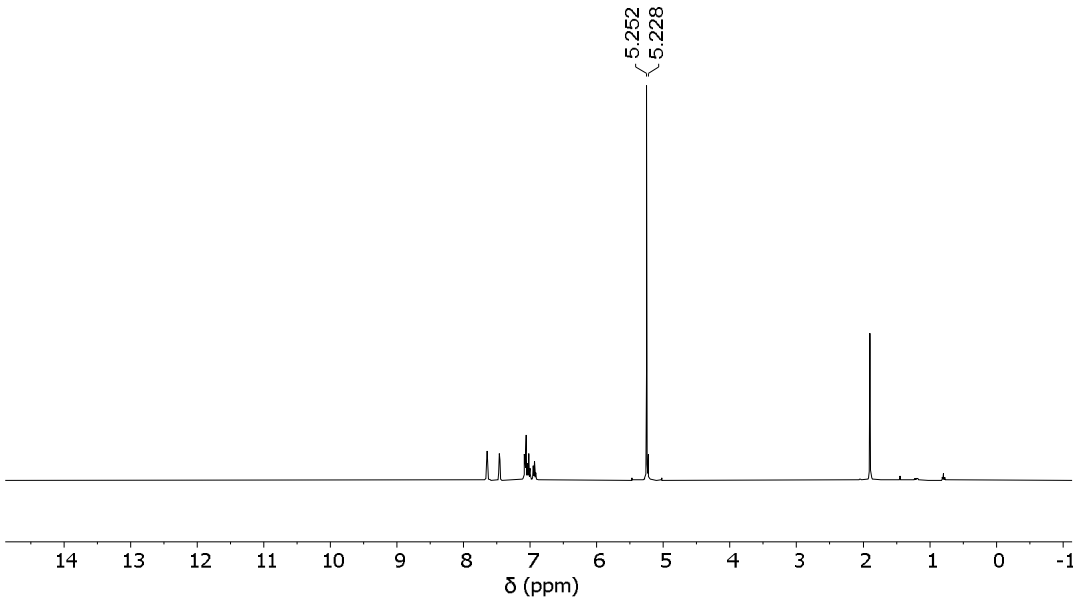

Figure S19. Evans method ^{1}H NMR spectrum of 20 mM solution of **6** in CD_2Cl_2. Magnetic moment: 1.31 μ_B.

Infrared Spectra

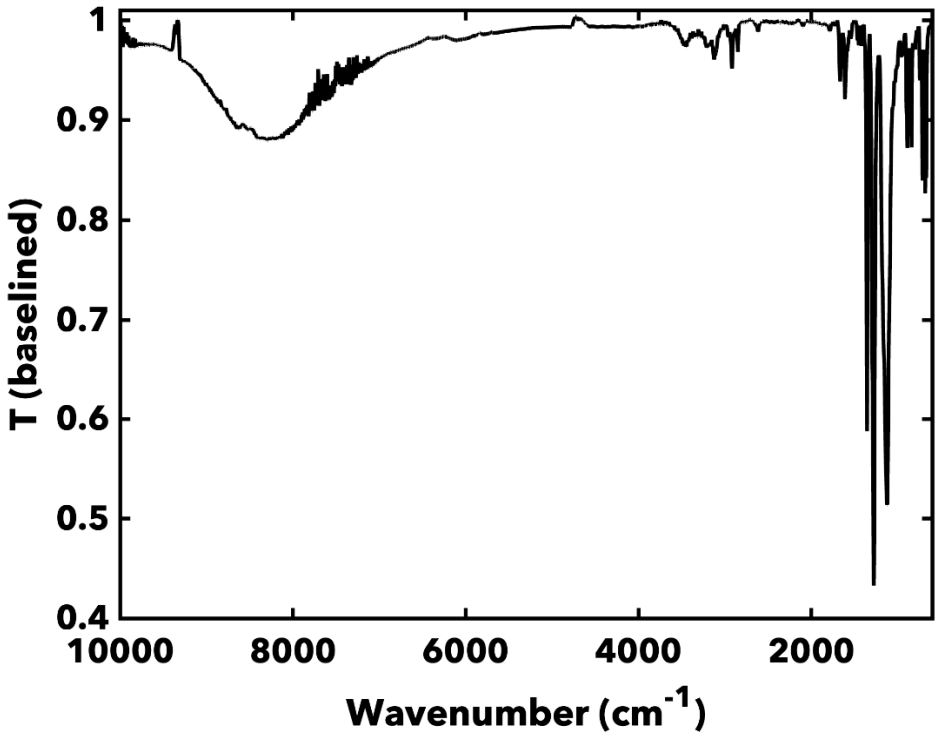

Figure S20. Infrared transmittance spectrum of a dropcast DCM solution of **1**.

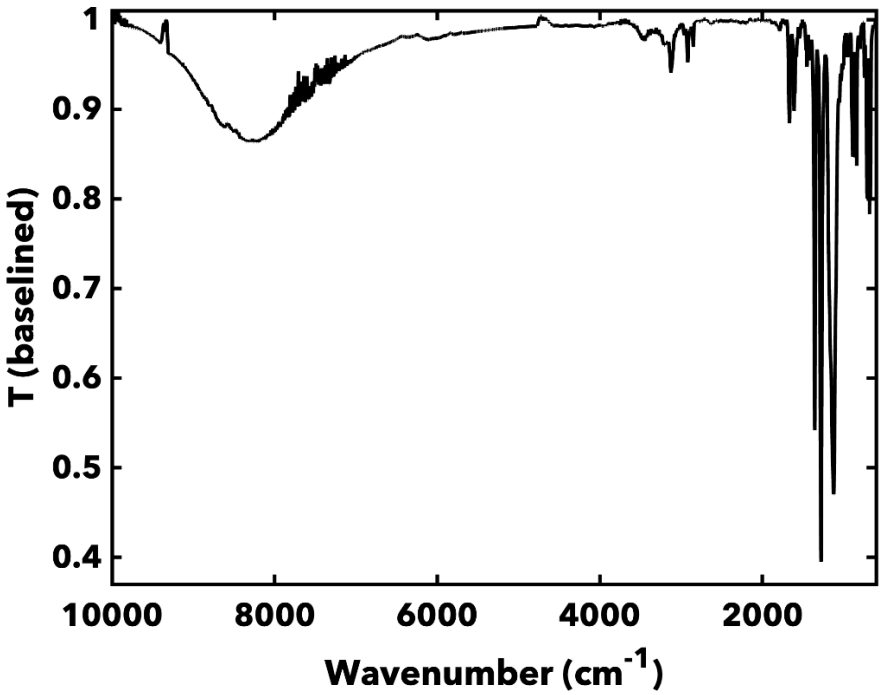

Figure S21. Infrared transmittance spectrum of a dropcast DCM solution of **2.**

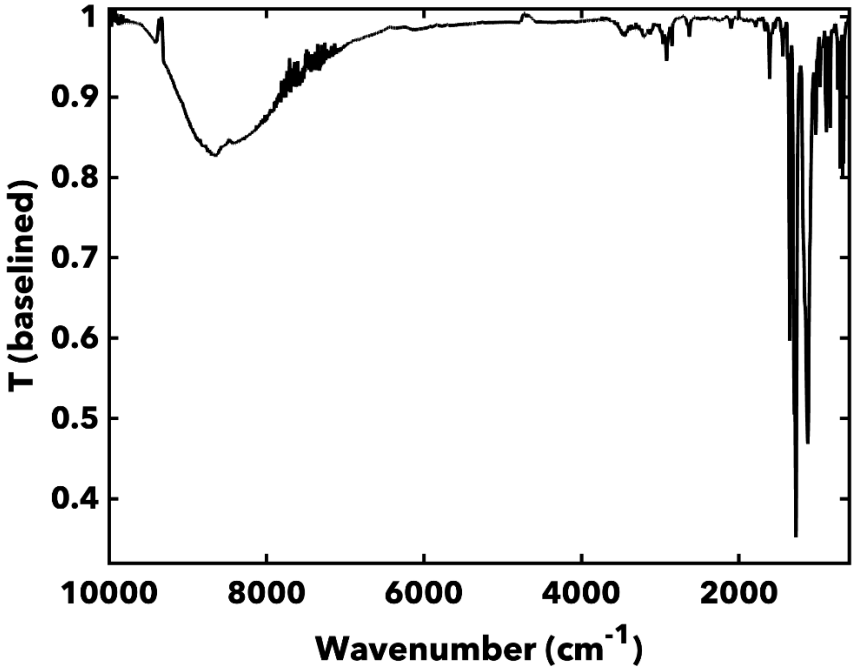

Figure S22. Infrared transmittance spectrum of a dropcast DCM solution of **3.**

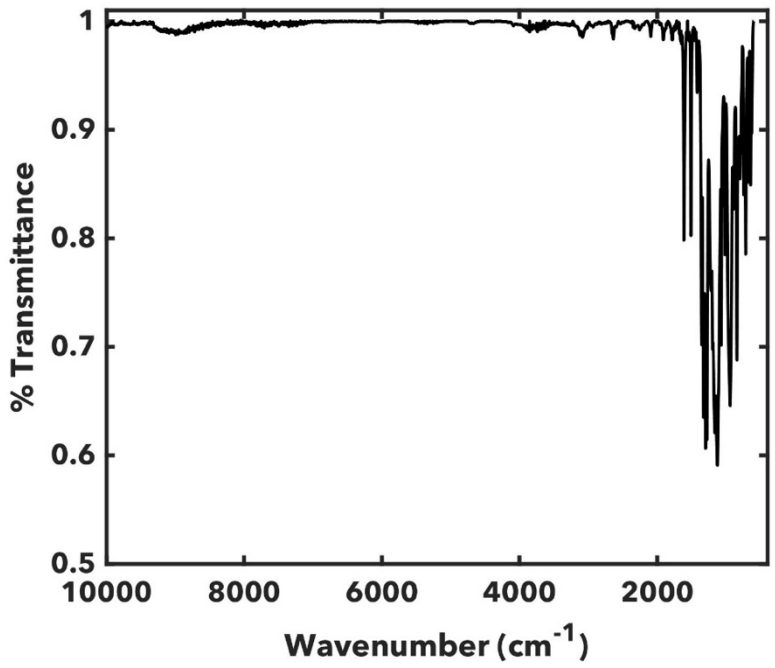

Figure S23. Infrared transmittance spectrum of a dropcast DCM solution of **4.**

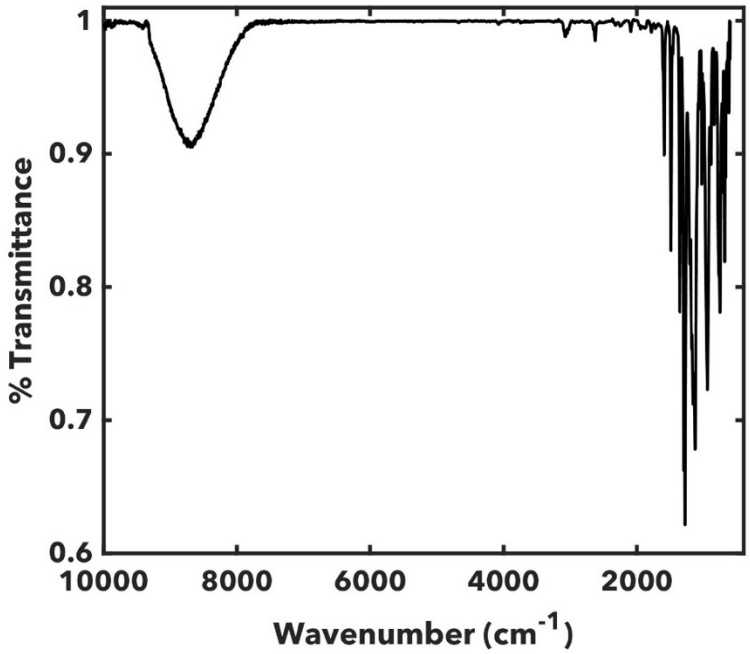

Figure S24. Infrared transmittance spectrum of a dropcast DCM solution of **5**.

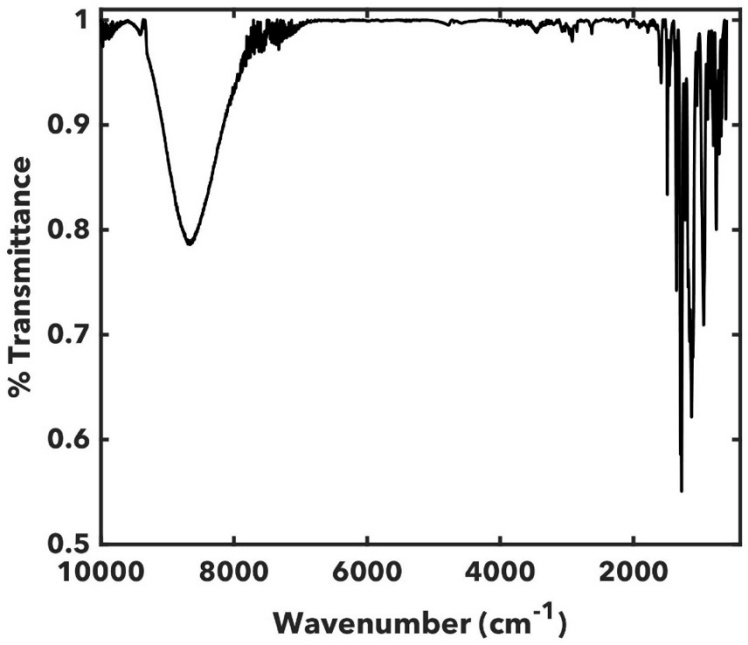

Figure S25. Infrared transmittance spectrum of a dropcast DCM solution of **6**.

Photoluminescence Quantum Yield

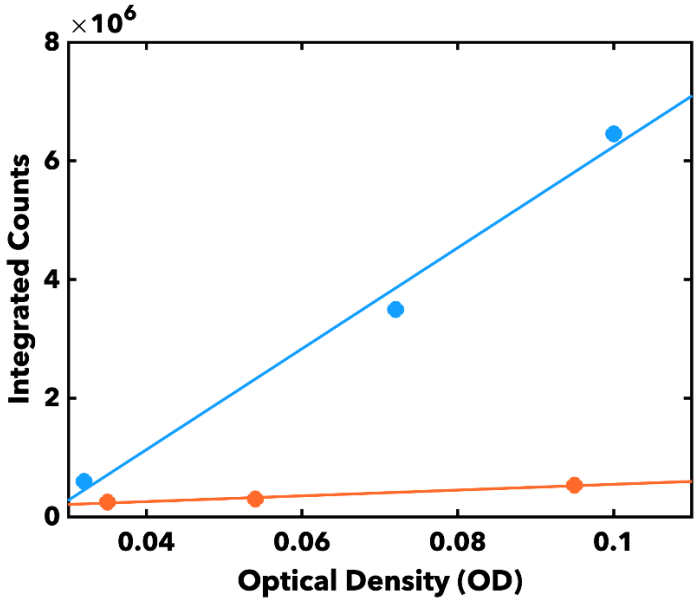

Figure S26. Photoluminescence quantum yield determinations for **1** in DCM at 298 K. $[(dppePt)_2TTFtt][BAr^F{}_4]_2$ in DCM (orange) at 298 K used as a standard reference.

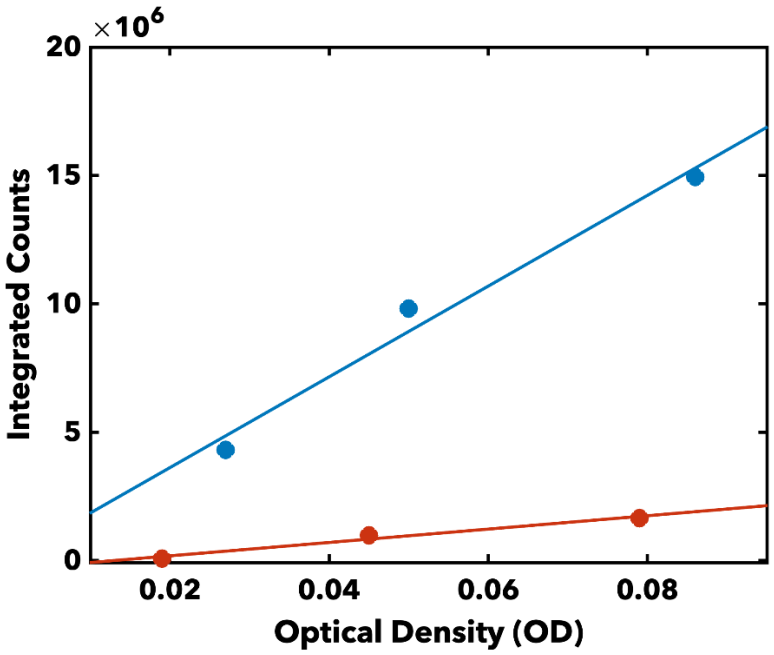

Figure S27. Photoluminescence quantum yield determinations for **2** in DCM at 298 K. $[(dppePt)_2TTFtt][BAr^F{}_4]_2$ in DCM (red) at 298 K used as a standard reference.

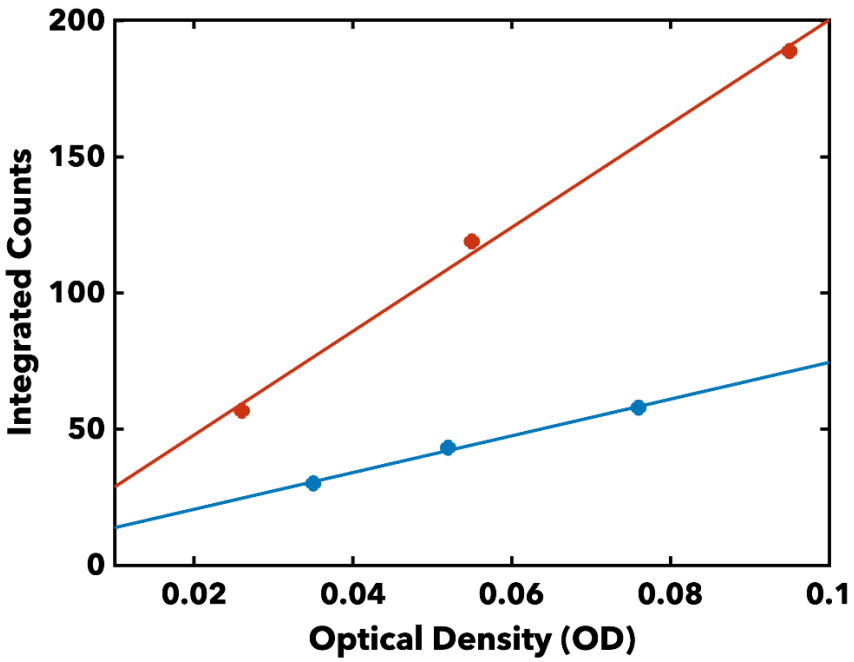

Figure S28. Photoluminescence quantum yield determinations for **3** in DCM at 298 K. $[(dppePt)_2TTFtt][BAr^F{}_4]_2$ in DCM (blue) at 298 K used as a standard reference.

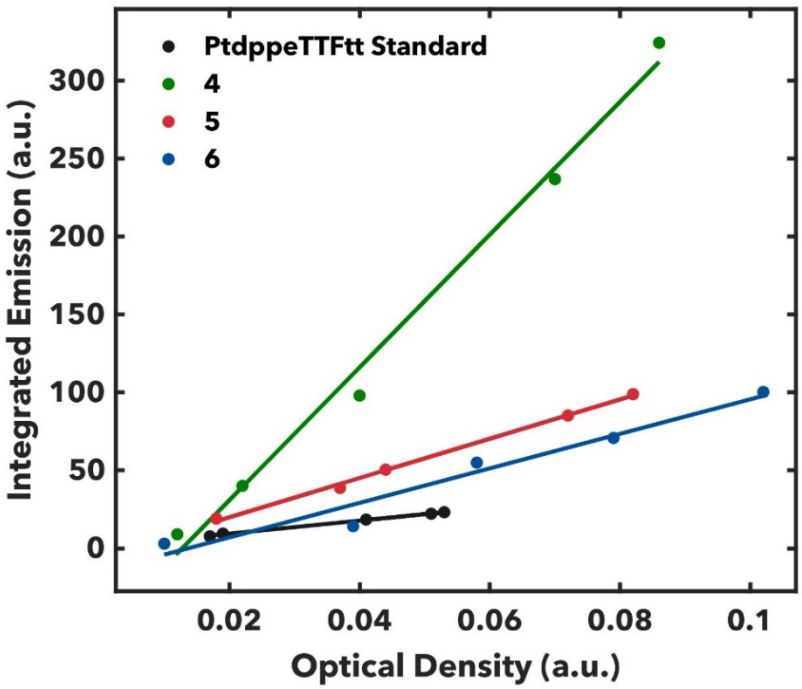

Figure S29. Photoluminescence quantum yield determinations for 4-6 in DCM at 298 K. $[(dppePt)_2TTFtt][BAr^F{}_4]_2$ in DCM at 298 K used as a standard reference.

Photoluminescence Spectra in CD_2Cl_2

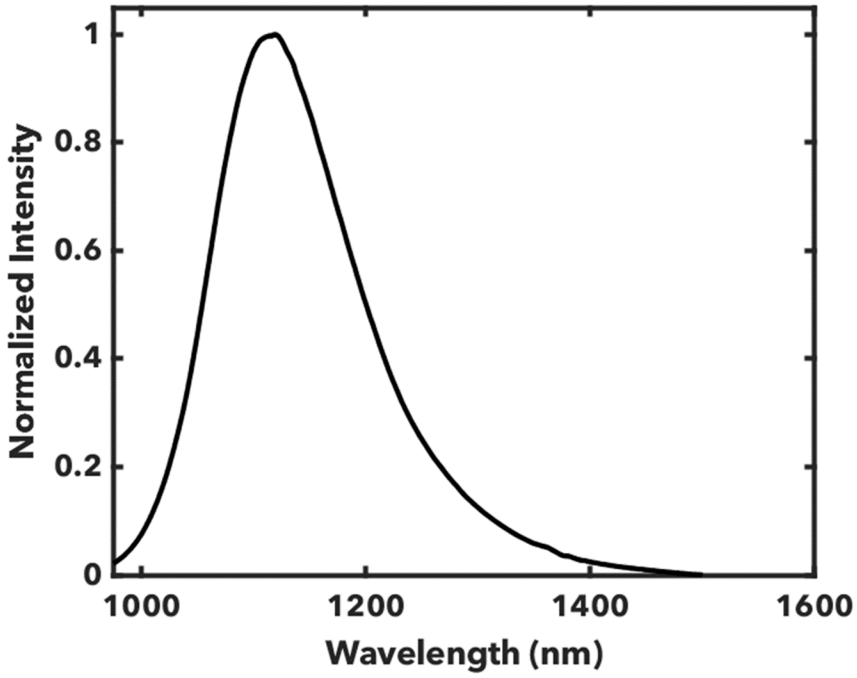

Figure S30. Photoluminescence spectrum of **3** in CD_2Cl_2.

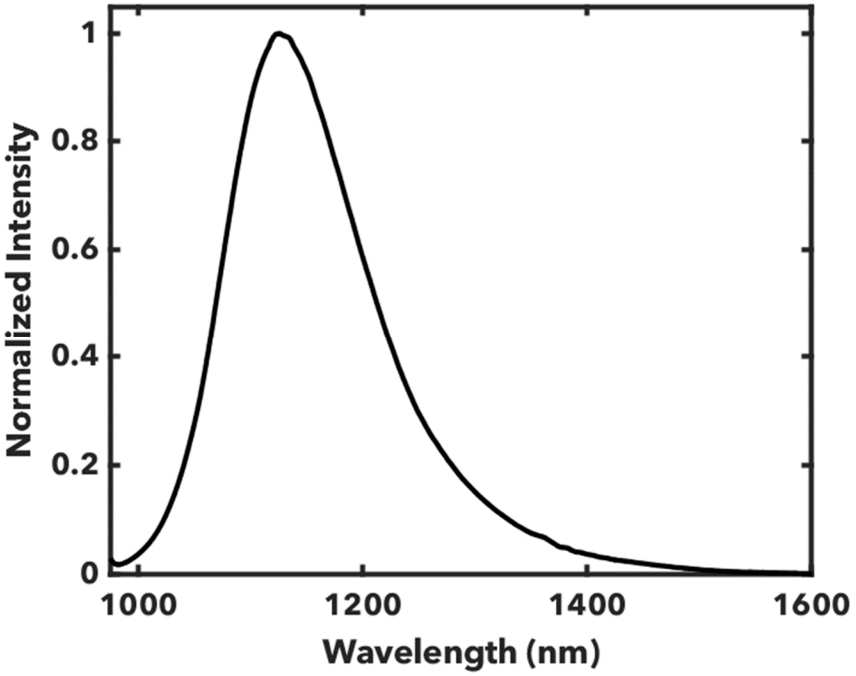

Figure S31. Photoluminescence spectrum of **5** in CD_2Cl_2.

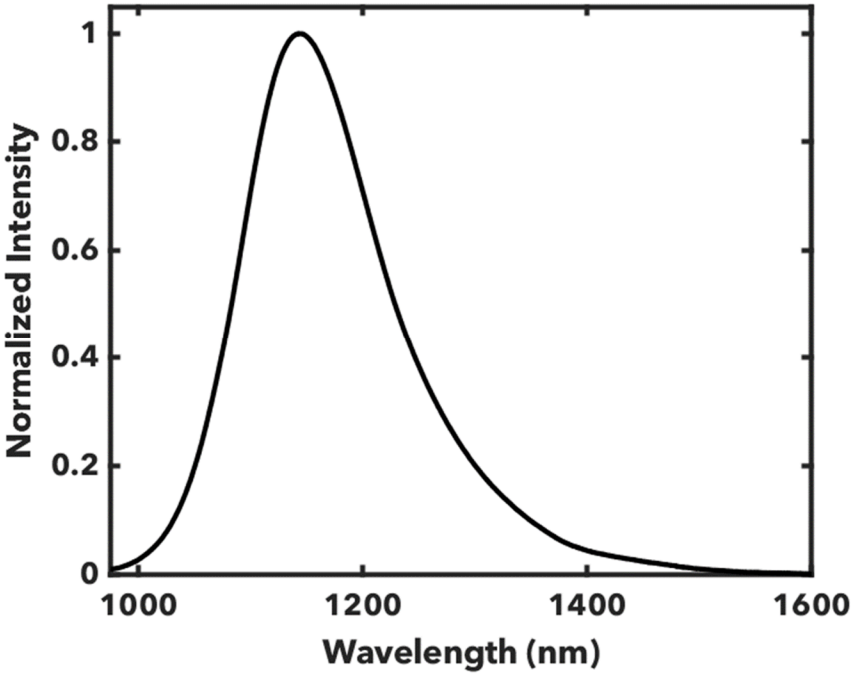

Figure S32. Photoluminescence spectrum of **6** in CD_2Cl_2.

Electron Paramagnetic Resonance (EPR) Spectra

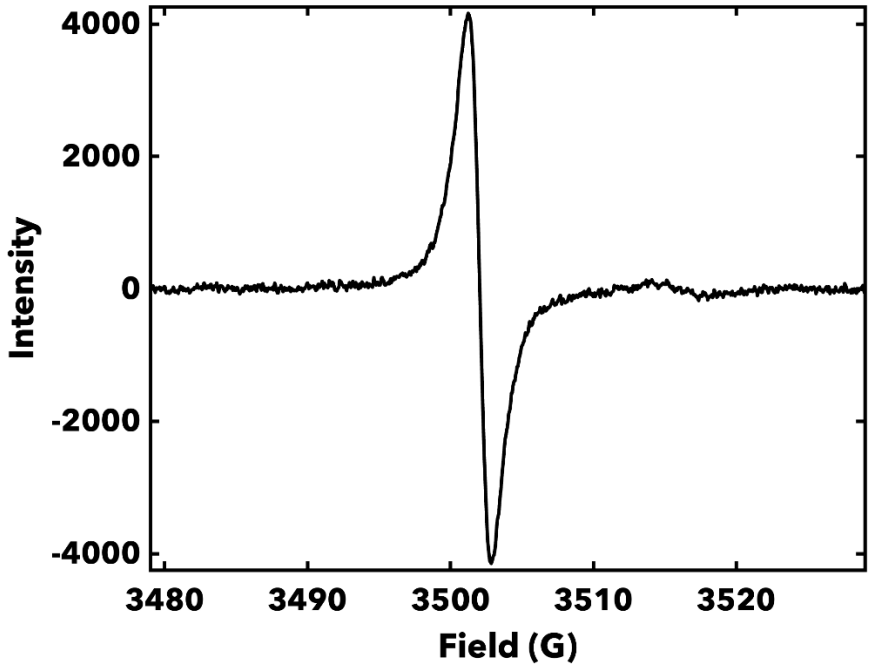

Figure S33. X-Band EPR spectrum of **1** in DCM at 298 K.

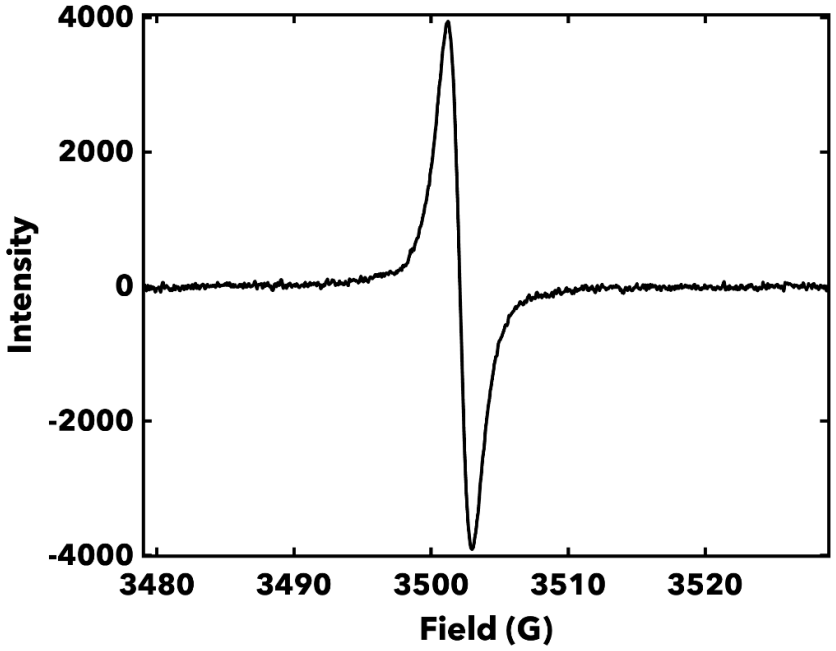

Figure S34. X-Band EPR spectrum of **2** in DCM at 298 K.

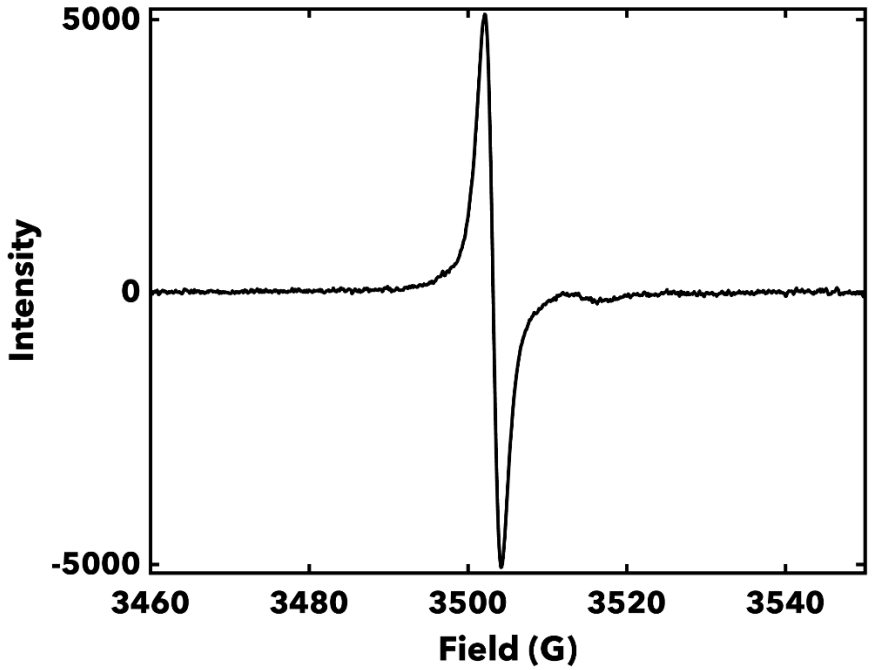

Figure S35. X-Band EPR spectrum of **3** in DCM at 298 K.

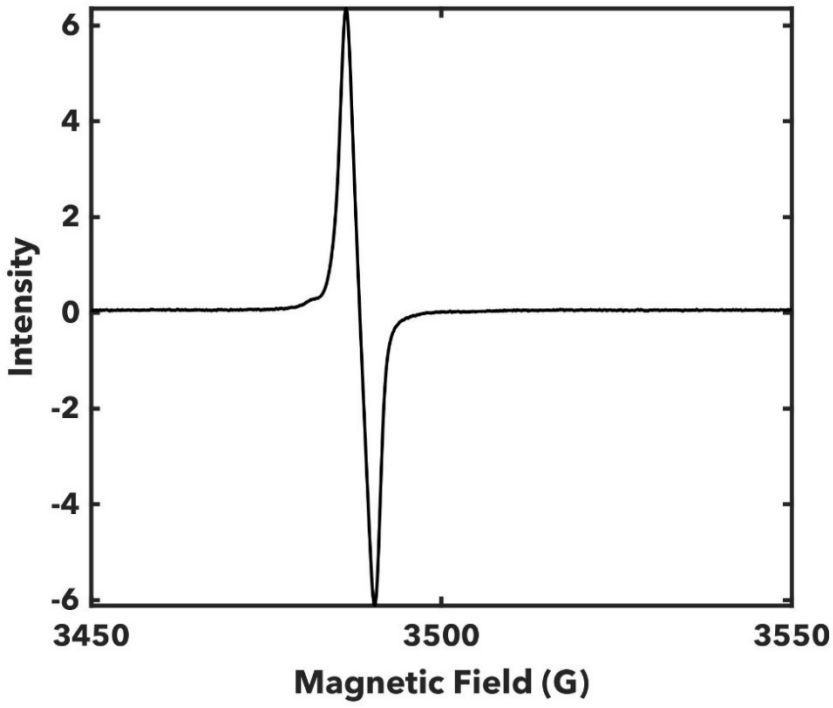

Figure S36. X-Band EPR spectrum of **4** in DCM at 298 K.

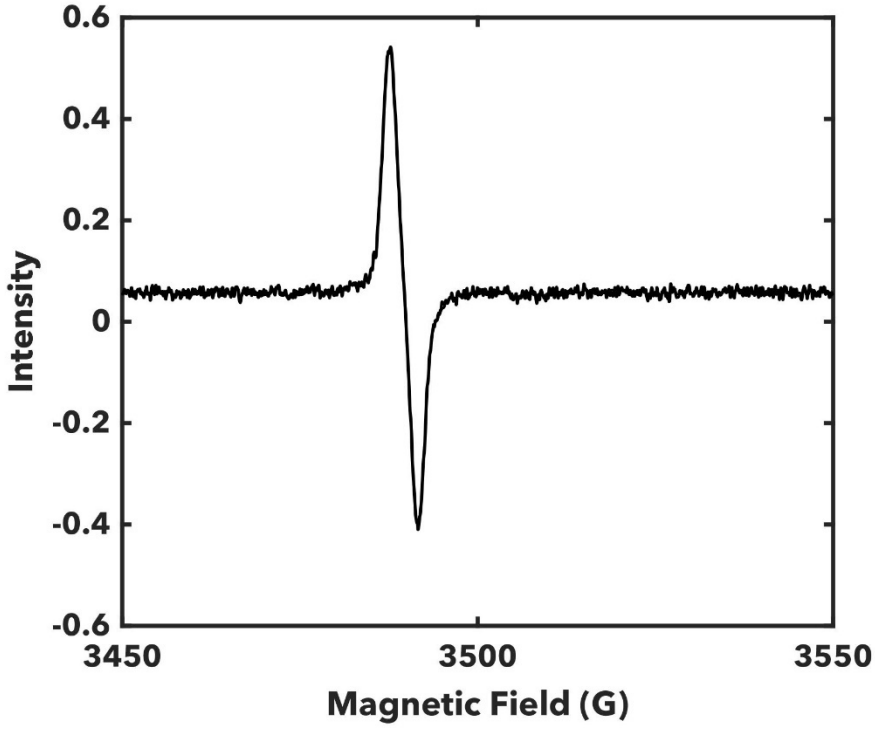

Figure S37. X-Band EPR spectrum of **5** in DCM at 298 K.

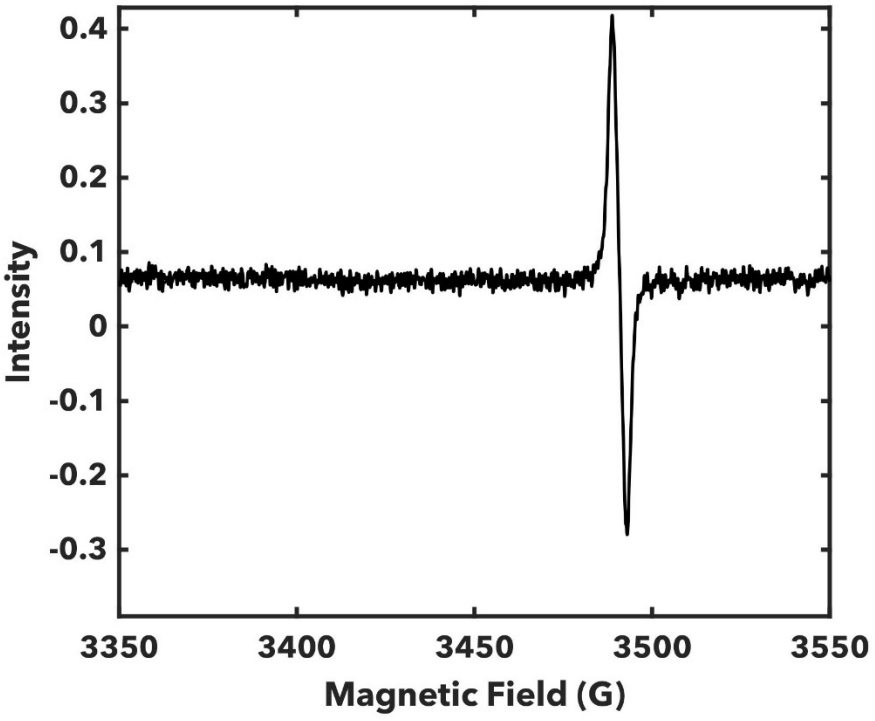

Figure S38. X-Band EPR spectrum of **6** in DCM at 298 K.

X-Ray Crystallographic Data

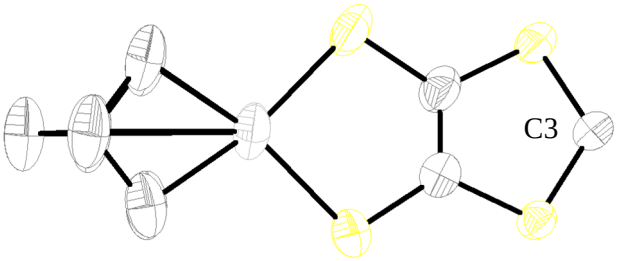

Figure S39. SXRD of asymmetric unit of **1**. Pt (silver), S (yellow), C (gray).
Selected bond lengths (Å): C3-C3': 1.41(2)

Table S1. SXRD of **1**.

Identification code	2377388
Empirical formula	$C_{84}H_{40}B_2F_{48}Pt_2S_8$
Formula weight	2629.89
Temperature/K	100(2)
Crystal system	triclinic
Space group	P-1
a/Å	12.4199(3)
b/Å	21.1332(5)
c/Å	21.2983(4)
α/°	77.134(2)
β/°	73.854(2)
γ/°	87.251(2)
Volume/Å^3	5234.3(2)
Z	2
ρ_{calc}g/cm^3	1.669
μ/mm^{-1}	2.955
F(000)	2540.0
Crystal size/mm^3	0.41 × 0.17 × 0.05
Radiation	Mo Kα (λ = 0.71073)
2Θ range for data collection/°	4.648 to 54
Index ranges	-15 ≤ h ≤ 15, -26 ≤ k ≤ 26, -27 ≤ l ≤ 27
Reflections collected	79602
Independent reflections	22772 [R_{int} = 0.0608, R_{sigma} = 0.0618]
Data/restraints/parameters	22772/7622/1907
Goodness-of-fit on F^2	1.079
Final R indexes [I>=2σ (I)]	R_1 = 0.1204, wR_2 = 0.2149
Final R indexes [all data]	R_1 = 0.1679, wR_2 = 0.2389
Largest diff. peak/hole / e Å^{-3}	5.03/-4.16

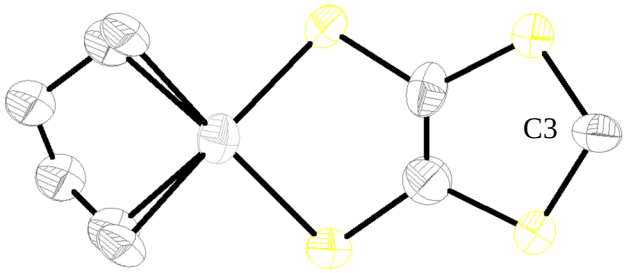

Figure S40. SXRD of asymmetric unit of **2**. Pt (silver), S (yellow), C (gray). Hydrogens, solvent, and counter anions omitted for clarity.

Selected bond lengths (Å): C3-C3': 1.44(3)

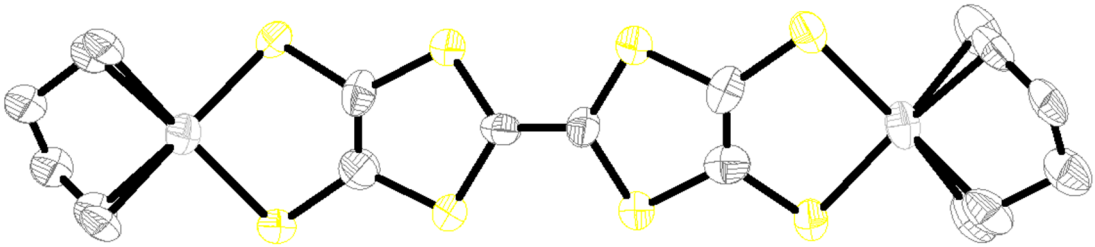

Figure S41. SXRD of entire molecule of **2** to show inversion symmetry. Pt (silver), S (yellow), C (gray). Hydrogens, solvent, and counter anions omitted for clarity.

Table S2. SXRD of **2**.

Identification code	2377387
Empirical formula	$C_{83}H_{46}B_2Cl_2F_{48}Pt_2S_8$
Formula weight	2694.38
Temperature/K	99.9(6)
Crystal system	triclinic
Space group	P-1
a/Å	12.7858(5)
b/Å	19.3482(6)
c/Å	20.0914(6)
α/°	81.874(3)
β/°	71.534(3)
γ/°	78.323(3)
Volume/Å^3	4600.8(3)
Z	2
ρ_{calc}g/cm^3	1.945
μ/mm^{-1}	9.151
F(000)	2608.0
Crystal size/mm^3	0.22 × 0.14 × 0.1
Radiation	Cu Kα (λ = 1.54184)
2Θ range for data collection/°	6.87 to 173.946

Index ranges	$-16 \leq h \leq 13$, $-24 \leq k \leq 24$, $-25 \leq l \leq 25$
Reflections collected	49286
Independent reflections	18715 [R_{int} = 0.1324, R_{sigma} = 0.0973]
Data/restraints/parameters	18715/2840/1406
Goodness-of-fit on F^2	1.108
Final R indexes [I>=2σ (I)]	R_1 = 0.1632, wR_2 = 0.3507
Final R indexes [all data]	R_1 = 0.1973, wR_2 = 0.3697
Largest diff. peak/hole / e $Å^{-3}$	6.65/-2.67

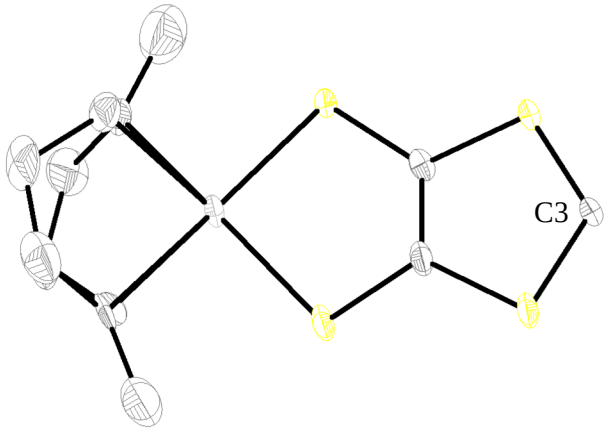

Figure S42. SXRD of asymmetric unit of **3**. Pt (silver), S (yellow), C (gray). Hydrogens, solvent, and counter anions omitted for clarity.

Selected bond lengths (Å): C3-C3': 1.42(1)

Table S3. SXRD of **3**.

Identification code	2377389
Empirical formula	$C_{90}H_{56}B_2F_{48}Pt_2S_8$
Formula weight	2717.62
Temperature/K	100(2)
Crystal system	monoclinic
Space group	$P2_1/n$
a/Å	13.4282(8)
b/Å	15.2001(9)
c/Å	24.6605(15)
α/°	90
β/°	103.9420(10)
γ/°	90
Volume/$Å^3$	4885.2(5)
Z	2
ρ_{calc}g/cm^3	1.848
μ/mm^{-1}	3.169
F(000)	2644.0
Crystal size/mm^3	0.178 × 0.115 × 0.082
Radiation	MoKα (λ = 0.71073)
2Θ range for data collection/°	3.902 to 57.07

Index ranges	$-18 \leq h \leq 18, -20 \leq k \leq 20, -33 \leq l \leq 33$
Reflections collected	197867
Independent reflections	12392 [R_{int} = 0.0812, R_{sigma} = 0.0407]
Data/restraints/parameters	12392/3/681
Goodness-of-fit on F^2	1.175
Final R indexes [I>=2σ (I)]	R_1 = 0.0691, wR_2 = 0.1292
Final R indexes [all data]	R_1 = 0.0893, wR_2 = 0.1397
Largest diff. peak/hole / e $Å^{-3}$	3.11/-2.71

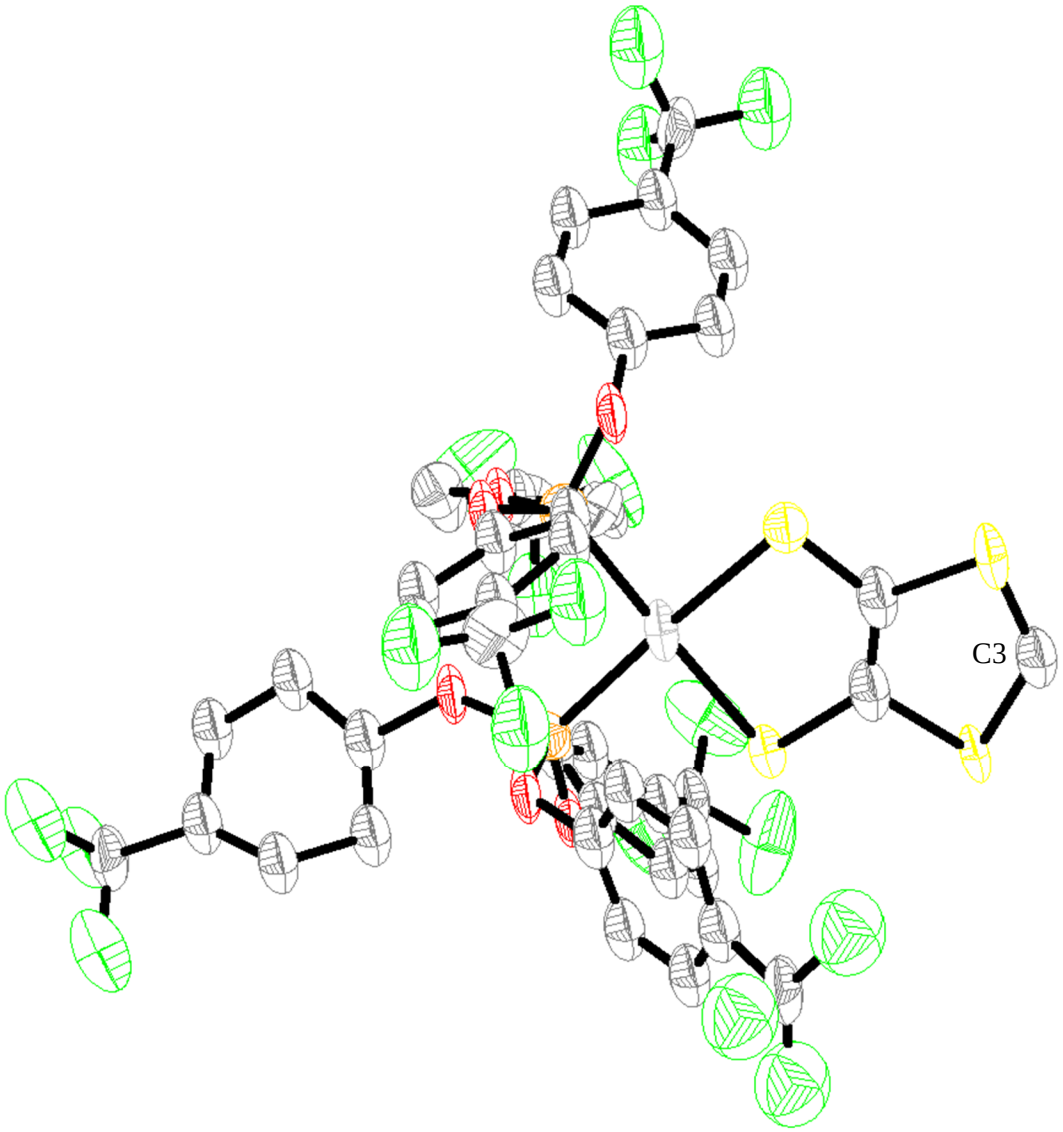

Figure S43. SXRD of asymmetric unit of **4**. Pt (silver), S (yellow), C (gray), P (orange), O (red), F (green). Hydrogens, solvent, and counter anions omitted for clarity.

Table S4. SXRD of **4**.

Identification code	2377391
Empirical formula	$C_{77}H_{35}BF_{42}O_6P_2PtS_4$
Formula weight	2250.13
Temperature/K	100(2)
Crystal system	triclinic
Space group	P-1
a/Å	14.630(4)
b/Å	15.470(4)
c/Å	19.500(5)
α/°	77.831(8)
β/°	78.221(8)
γ/°	79.506(9)
Volume/Å^3	4178.5(19)
Z	2
ρ_{calc}g/cm^3	1.788
μ/mm^{-1}	1.963
F(000)	2200.0
Crystal size/mm^3	0.243 × 0.112 × 0.073
Radiation	MoKα (λ = 0.71073)
2Θ range for data collection/°	3.66 to 46.806
Index ranges	$-16 \leq h \leq 16$, $-17 \leq k \leq 17$, $-21 \leq l \leq 21$
Reflections collected	64722
Independent reflections	12109 [R_{int} = 0.1299, R_{sigma} = 0.1042]
Data/restraints/parameters	12109/3567/788
Goodness-of-fit on F^2	1.077
Final R indexes [I>=2σ (I)]	R_1 = 0.2214, wR_2 = 0.5152
Final R indexes [all data]	R_1 = 0.2834, wR_2 = 0.5530
Largest diff. peak/hole / e Å^{-3}	6.17/-2.34

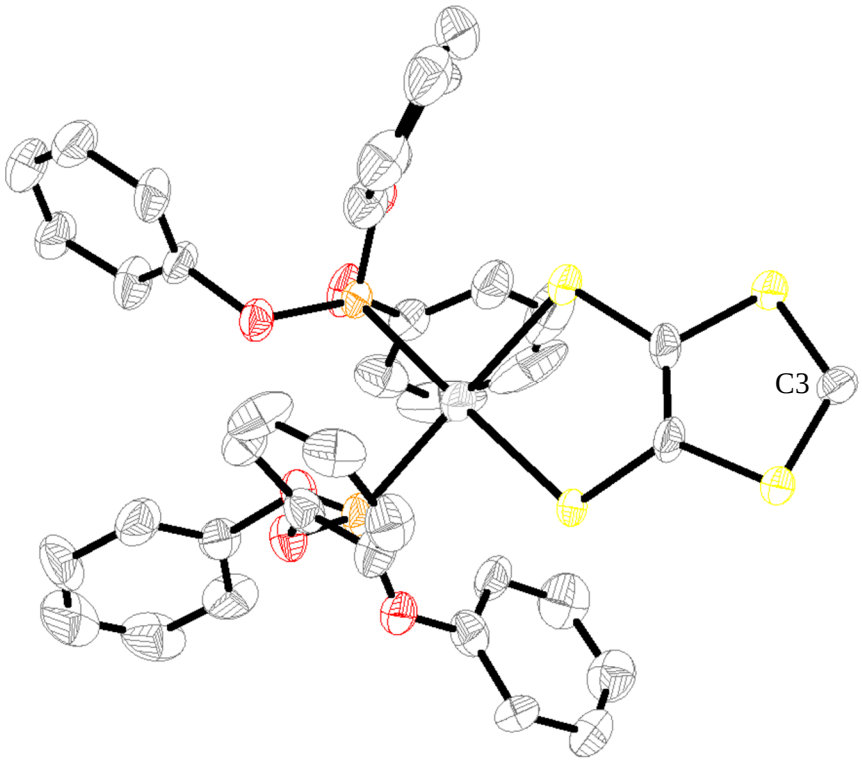

Figure S44. SXRD of asymmetric unit of **5**. Pt (silver), S (yellow), C (gray), P (orange), O (red). Hydrogens, solvent, and counter anions omitted for clarity.

Selected bond lengths (Å): C3-C3': 1.38(2)

Table S5. SXRD of **5**.

Identification code	2377390
Empirical formula	$C_{142}H_{84}B_2F_{48}O_{12}P_4Pt_2S_8$
Formula weight	3686.25
Temperature/K	100(2)
Crystal system	monoclinic
Space group	$P2_1/c$
a/Å	17.3397(12)
b/Å	24.6986(18)
c/Å	18.9907(14)
α/°	90
β/°	116.819(2)
γ/°	90
Volume/Å^3	7258.2(9)
Z	2
ρ_{calc}g/cm^3	1.687
μ/mm^{-1}	2.206
F(000)	3636.0
Crystal size/mm^3	0.143 × 0.063 × 0.046

Radiation	MoKα (λ = 0.71073)
2Θ range for data collection/°	4.08 to 49.442
Index ranges	-20 ≤ h ≤ 20, -28 ≤ k ≤ 28, -22 ≤ l ≤ 22
Reflections collected	111620
Independent reflections	12350 [R_{int} = 0.0970, R_{sigma} = 0.0668]
Data/restraints/parameters	12350/585/909
Goodness-of-fit on F^2	1.179
Final R indexes [I>=2σ (I)]	R_1 = 0.0772, wR_2 = 0.1904
Final R indexes [all data]	R_1 = 0.1491, wR_2 = 0.2677
Largest diff. peak/hole / e $Å^{-3}$	4.30/-2.30

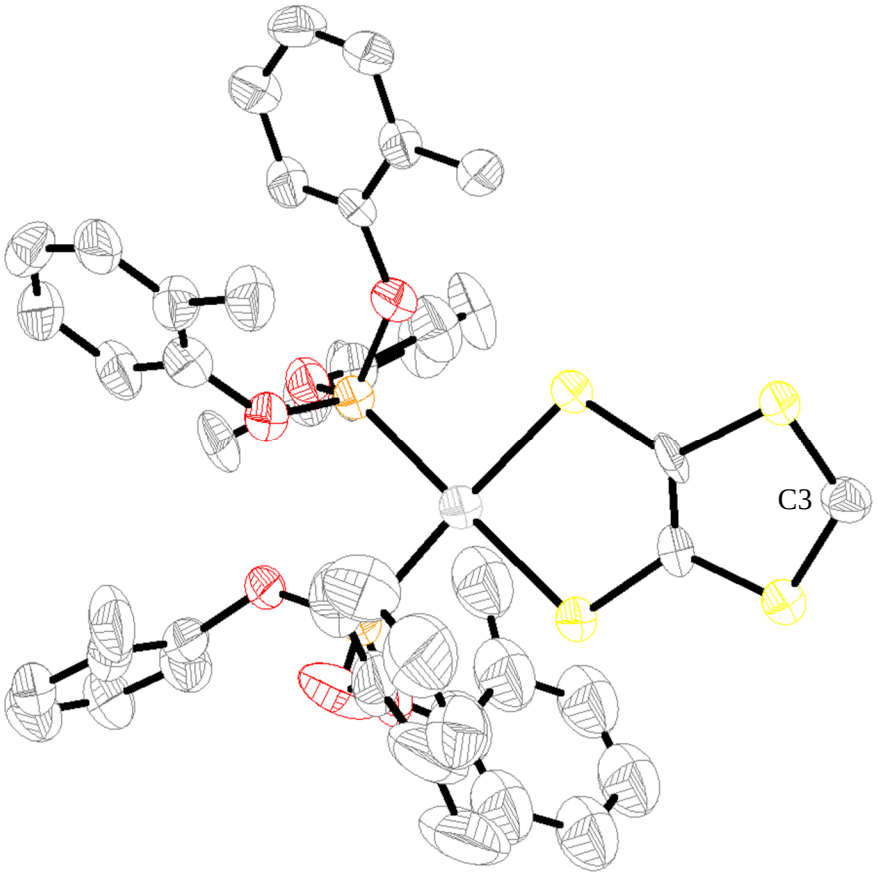

Figure S45. SXRD of **6**. Pt (silver), S (yellow), C (gray), P (orange), O (red). Hydrogens, solvent, and counter anions omitted for clarity.

Selected bond lengths (Å): C3-C3': 1.39(2)

Table S6. SXRD of **6**.

Identification code	2377392
Empirical formula	$C_{77}H_{54}BF_{24}O_6P_2PtS_4$
Formula weight	1927.28

Temperature/K	100(2)
Crystal system	monoclinic
Space group	$P2_1/n$
a/Å	26.9879(15)
b/Å	21.3132(11)
c/Å	29.4717(16)
α/°	90
β/°	99.619(2)
γ/°	90
Volume/Å^3	16713.7(16)
Z	8
ρ_{calc}g/cm^3	1.532
μ/mm^{-1}	1.920
F(000)	7656.0
Crystal size/mm^3	0.126 × 0.086 × 0.075
Radiation	MoKα (λ = 0.71073)
2Θ range for data collection/°	3.524 to 49.49
Index ranges	$-31 \leq h \leq 31$, $-25 \leq k \leq 25$, $-34 \leq l \leq 34$
Reflections collected	388919
Independent reflections	28557 [R_{int} = 0.1068, R_{sigma} = 0.0633]
Data/restraints/parameters	28557/3432/1924
Goodness-of-fit on F^2	1.441
Final R indexes [I>=2σ (I)]	R_1 = 0.1272, wR_2 = 0.3053
Final R indexes [all data]	R_1 = 0.2169, wR_2 = 0.4029
Largest diff. peak/hole / e Å^{-3}	13.23/-2.99

Computational Information

Computational Methods

All geometry optimizations performed in Orca 5.0.2[10] using the PBE0 functional.[11] Additionally, these optimizations use the RIJCOSX approximation and were held to TIGHTSCF convergence criteria. The ZORA relativistic correction was used and the SARC-ZORA-TZVP basis set was used for Pt and ZORA-def2-SVP basis set for all other atoms.[12,13] The SARC/J auxiliary basis set on all atoms.[12,14] Grimme's dispersion correction with Becke-Johnson damping was also used.[15,16]

All natural bonding orbital (NBO) analyses were performed using the NBO 6.0[17] package in Gaussian 09 Revision D.01.[18] For these calculations, we employed the B3LYP functional and the SDDAll basis set on all atoms. Additionally, we applied the Grimme's dispersion correction with Becke-Johnson damping[15,16] and the Douglas-Kroll-Hess 2nd order relativistic correction.[19,20]

2nd Order Perturbative Energy Analysis

Natural bonding orbital analysis was performed on the $PtCl_2L_{(2)}$ fragment of **1-6** in addition to select phosphine-capped Pt-TTFtt complexes as previously reported by our laboratory.[21] The backbonding interaction for **1-6** and the phosphine analogs are reported in **Table S7**, however, σ interactions could not be calculated for the phosphines. We found that in compounds **1-6**, the P lone pair donates into the Pt-Cl σ* orbital in which case a 2nd order interaction could be calculated. However, in the case of the phosphines,

the Pt-P bond becomes lower in energy than the Pt-Cl bond, so instead we find that the Cl lone pair donates into the Pt-P σ*. Because of this, we performed a linear regression on the weighted average of backbonding and σ interaction contributions for only the compounds **1-6** according to the following equation:

$$A_{fit} = a\,\pi_b + (1-a)\sigma + c$$

When doing so with compounds **1-6**, the *p*-CF_3 analog stands out as a possible outlier. Performing the appropriate statistical analysis confirms that **4** lies outside one standard deviation from expectation. Previously reported *p*-CF_3 analogs also behaved distinctly from similar compounds likely due to fluorophilic interactions between it and the $BAr^F{}_4$ counteranions, so removing **4** from the fit is acceptable.[21] After removing **4**, we find that the R^2 improves from 0.52 to 0.93, and the weight changes from a roughly equal contribution from π_b and σ to becoming dominated by π_b (from a = 0.58 to a = 0.79) (**Fig. S43**). While backbonding interactions seem to dominate in modulating absorption maximum, it alone is insufficient as a predictor. Similar statistical analysis was performed with emission. However, in this case, no satisfactory trend was observed, the best weight yielded a fit with R^2 = 0.42. Additionally, both **4** and **6** exhibited behavior more than one standard deviation from the mean (**Fig. S44**). The lack of concrete trend with emission may be ascribed to convolutions from solvent absorptions and/or some excited state reorganization. When plotting backbonding against absorption and emission maximum for **1-6** along with **L** = 1,2-bis(diphenylphosphino) ethane (dppe), PPh_3, P(*p*-BrPh)$_3$, and P(*p*-OMePh)$_3$, we find that there is no clear trend (**Fig. S45**).[6,21] Instead, there are two groups of points: P-based ligands and olefins, suggesting that backbonding alone is insufficient in determining photophysical properties. A rough trend is observed when only considering the P-based ligands' backbonding and absorption/emission maxima (**Fig. S46**). Thus, to create a general model that is consistent among P-based ligands with olefins, we consider some σ contributions. When doing so, we find a satisfactory trend.

Table S7. Computed backbonding and σ donation values and photophysical parameters for compounds **1-6** and select phosphine-capped PtTTFtt complexes previously reported. [a] Values taken from fluorescence spectrum collected in CD_2Cl_2

	1	**2**	**3**	**4**	**5**	**6**	dppe	P(*p*-OMePh)$_3$	PPh_3	P(p-BrPh)$_3$
π_b (kcal/mol)	109	100	96	37	40	37	33	27	28	28
σ (kcal/mol)	580	559	551	587	556	617	-------	-------	-------	-------
λ_{Abs} (nm)	890	914	975	931	984	1005	1044	1130	1100	1059
E_{Abs} (eV)	1.394	1.357	1.272	1.332	1.261	1.234	1.188	1.098	1.128	1.171
λ_{Em} (nm)	1030	1059	1115[a]	1064	1127[a]	1143[a]	1202	1280	1266	1198
E_{em}(eV)	1.204	1.171	1.113	1.165	1.101	1.085	1.032	0.969	0.980	1.036

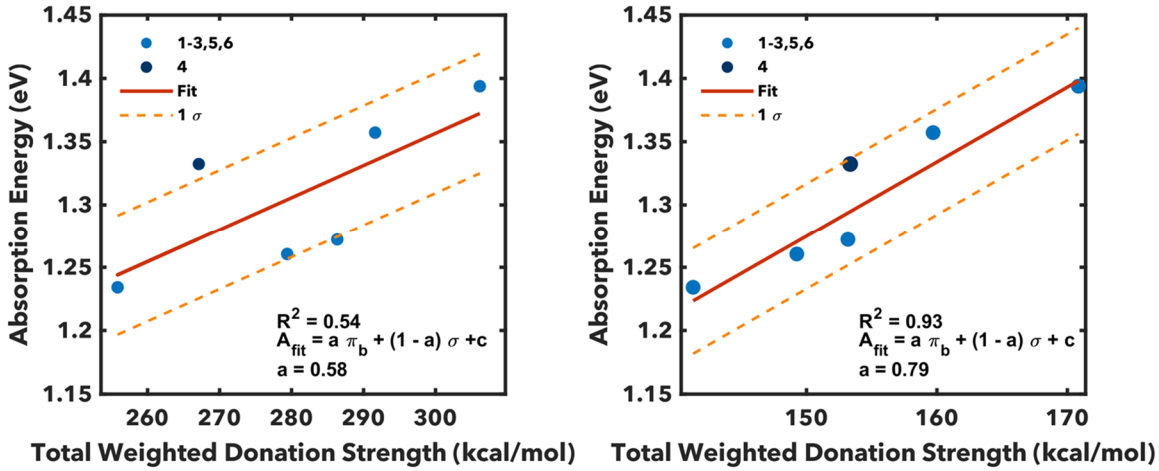

Figure S46. Weighted absorption fit with 1 standard deviation. Fit including **4** (left) and excluding **4** as an outlier (right).

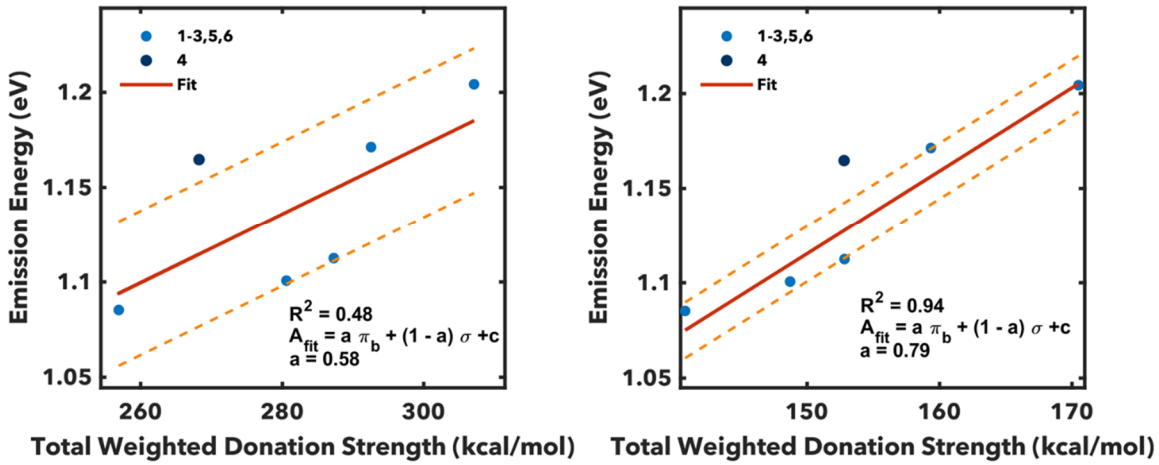

Figure S47. Weighted emission energy fit with 1 standard deviation. Fit including **4** (left) and excluding **4** as an outlier (right).

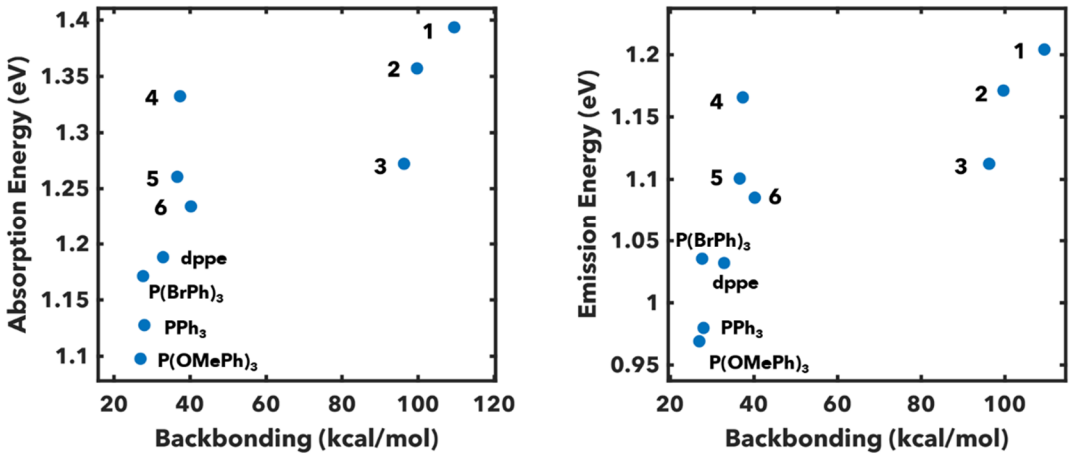

Figure S48. Absorption (left) and emission (right) of compounds **1**-**6** and select phosphine-capped PtTTFtt compounds plotted against only computed backbonding strength.

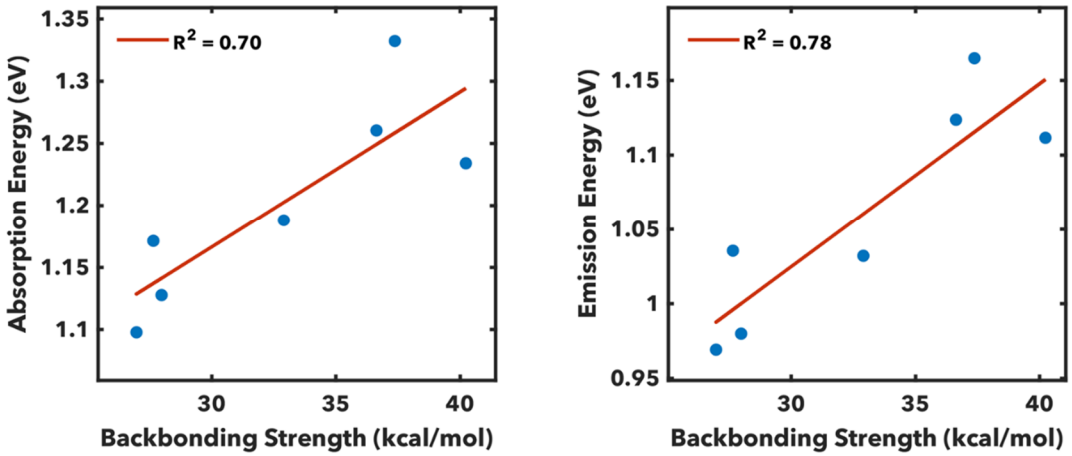

Figure S49. Absorption (left) and emission (right) of P-based ligands against computed backbonding (**4**-**6** and phosphine-capped PtTTFtt compounds) and a linear fit.

References

1 J. Xie, J.-N. Boyn, A. S. Filatov, A. J. McNeece, D. A. Mazziotti and J. S. Anderson, *Chem. Sci.*, 2020, **11**, 1066–1078.

2 Y. D. Bidal, C. A. Urbina-Blanco, A. Poater, D. B. Cordes, A. M. Z. Slawin, L. Cavallo and C. S. J. Cazin, *Dalton Trans.*, 2019, **48**, 11326–11337.

3 A. L. Fuller, F. R. Knight, A. M. Z. Slawin and J. D. Woollins, *Eur. J. Inorg. Chem.*, 2010, **2010**, 4034–4043.

4 A. Lüning, M. Neugebauer, V. Lingen, A. Krest, K. Stirnat, G. B. Deacon, P. R. Drago, I. Ott, J. Schur, I. Pantenburg, G. Meyer and A. Klein, *Eur. J. Inorg. Chem.*, 2015, **2015**, 226–239.

5 Diamagnetic Corrections and Pascal's Constants | Journal of Chemical Education, https://pubs.acs.org/doi/10.1021/ed085p532, (accessed 27 August 2024).

6 L. E. McNamara, J.-N. Boyn, C. Melnychuk, S. W. Anferov, D. A. Mazziotti, R. D. Schaller and J. S. Anderson, *J. Am. Chem. Soc.*, 2022, **144**, 16447–16455.

7 G. M. Sheldrick, *Acta Crystallographica Section C*, 2015, **71**, 3–8.

8 O. V. Dolomanov, L. J. Bourhis, R. J. Gildea, J. A. K. Howard and H. Puschmann, *J. Appl. Cryst.*, 2009, **42**, 339–341.

9 G. M. Sheldrick, *Acta Cryst A*, 2008, **64**, 112–122.

10 F. Neese, *WIREs Computational Molecular Science*, 2022, **12**, e1606.

11 C. Adamo and V. Barone, *J. Chem. Phys.*, 1999, **110**, 6158–6170.

12 D. A. Pantazis, X.-Y. Chen, C. R. Landis and F. Neese, *J. Chem. Theory Comput.*, 2008, **4**, 908–919.

13 F. Weigend and R. Ahlrichs, *Phys. Chem. Chem. Phys.*, 2005, **7**, 3297–3305.

14 F. Weigend, *Phys. Chem. Chem. Phys.*, 2006, **8**, 1057–1065.

15 S. Grimme, J. Antony, S. Ehrlich and H. Krieg, *J. Chem. Phys.*, 2010, **132**, 154104.

16 S. Grimme, S. Ehrlich and L. Goerigk, *J. Comp. Chem.*, 2011, **32**, 1456–1465.

17 NBO 6.0 E. D. Glendening, J. K. Badenhoop, A. E. Reed, J. E. Carpenter, J. A. Bohmann, C. M. Morales, C. R. Landis, and F. Weinhold (Theoretical Chemistry Institute, University of Wisconsin, Madison, WI, 2013); http://nbo6.chem.wisc.edu/, .

18 Gaussian 09, Revision D.01, M. J. Frisch, G. W. Trucks, H. B. Schlegel, G. E. Scuseria, M. A. Robb, J. R. Cheeseman, G. Scalmani, V. Barone, B. Mennucci, G. A. Petersson, H. Nakatsuji, M. Caricato, X. Li, H. P. Hratchian, A. F. Izmaylov, J. Bloino, G. Zheng, J. L. Sonnenberg, M. Hada, M. Ehara, K. Toyota, R. Fukuda, J. Hasegawa, M. Ishida, T. Nakajima, Y. Honda, O. Kitao, H. Nakai, T. Vreven, J. A. Montgomery, Jr., J. E. Peralta, F. Ogliaro, M. Bearpark, J. J. Heyd, E. Brothers, K. N. Kudin, V. N. Staroverov, T. Keith, R. Kobayashi, J. Normand, K. Raghavachari, A. Rendell, J. C. Burant, S. S. Iyengar, J. Tomasi, M. Cossi, N. Rega, J. M. Millam, M. Klene, J. E. Knox, J. B. Cross, V. Bakken, C. Adamo, J. Jaramillo, R. Gomperts, R. E. Stratmann, O. Yazyev, A. J. Austin, R. Cammi, C. Pomelli, J. W. Ochterski, R. L. Martin, K. Morokuma, V. G. Zakrzewski, G. A. Voth, P. Salvador, J. J. Dannenberg, S. Dapprich, A. D. Daniels, O. Farkas, J. B. Foresman, J. V. Ortiz, J. Cioslowski, and D. J. Fox, Gaussian, Inc., Wallingford CT, 2013.

19 M. Douglas and N. M. Kroll, *Annals of Physics*, 1974, **82**, 89–155.

20 G. Jansen and B. A. Hess, *Phys. Rev. A*, 1989, **39**, 6016–6017.

21 L. E. McNamara, J.-N. Boyn, S. W. Anferov, A. S. Filatov, M. W. Maloney, D. A. Mazziotti, R. D. Schaller and J. S. Anderson, *J. Am. Chem. Soc.*, 2024, **146**, 17285–17295.